EUROPEAN ORGANIZATION FOR NUCLEAR

STUDIES OF PROTON-PROTON COLLISIONS AT THE CERN ISR WITH AN IDENTIFIED CHARGED HADRON OF HIGH TRANSVERSE MOMENTUM AT 90°

II. ON THE DISTRIBUTION OF CHARGED PARTICLES IN THE CENTRAL REGION

M.G. Albrow[1], S. Almehed[2], P.S.L. Booth[3], X. de Bouard[4], H. Bøggild[5], L.J. Carroll[3], P. Catz[4], E. Dahl-Jensen[5], I. Dahl-Jensen[5], G. Damgaard[5], G. von Dardel[2], N. Elverhaug[6], K.H. Hansen[5], J.N. Jackson[3], G. Jancso[4*], G. Jarlskog[2], H.B. Jensen[5], L. Jönsson[2], A. Klovning[6], E. Lillethun[6], A. Lu[4], B. Lörstad[2], N.A. McCubbin[1], H.E. Miettinen[5], J.V. Morris[3], R. Møller[5], S.Ø. Nielsen[5], J.O. Petersen[5], J.A.J. Skard[6] and P. Villeneuve[7]

British-French-Scandinavian Collaboration

1) Rutherford Laboratory, Chilton, Didcot, United Kingdom

2) University of Lund, Sweden

3) University of Liverpool, United Kingdom

4) Laboratoire d'Annecy-le-Vieux de Physique des Particules, Annecy, France

5) Niels Bohr Institute, Copenhagen, Denmark

6) University of Bergen, Norway

7) LPNHE, University of Paris VI, Paris, France

Geneva - 25 July 1978

(Submitted to Nuclear Physics B)

---

*) Now at the Central Research Institute for Physics, Hungarian Academy of Sciences, Budapest.

ABSTRACT

Results are reported from an investigation of proton-proton collisions at a c.m. energy of 52.6 GeV, in which a charged hadron with large transverse momentum is produced near 90° in the c.m.s. We have studied the momentum and charge correlations between identified high p_T trigger particles and other charged particles in the central region (rapidity $|y| < 3$). When the momentum of the trigger particle is increased, we observe an increase of the density of high p_T particles with charge opposite to that of the trigger particle in a small solid angle around the trigger particle. The sum of the momenta of charged particles inside $|y| < 1$, following the trigger particle, is found to increase by 35 ± 6 MeV/c per GeV/c increase of the trigger momentum. Opposite in azimuth to the trigger particle we observe close pairs of high p_T particles in both neutral and doubly charged combinations. In this region we see an indication of scaling in the x_E variable for trigger momenta exceeding 3 GeV/c. The distribution of charge is strongly correlated with the charge of the trigger particle. Otherwise the type of trigger particle does not affect strongly the observed event structure, but for trigger momenta above 3 GeV/c K^- and $\bar{p}$ triggers are observed to have fewer negative high p_T recoil particles within $|y| < 1$ than other trigger particles.

1. INTRODUCTION

The small fraction of high-energy proton-proton collisions in which one or more particles with large transverse momentum, p_T, are produced, is a promising source of information about the interaction between constituents of the two protons. Several experiments [1-4] indicate that a large transverse momentum is frequently carried by a group of particles moving in similar directions, a so-called "jet", balanced by another group of particles roughly opposite in azimuth. In some theoretical models [5-11] such jets are interpreted as resulting from the fragmentation of scattered constituents of the colliding protons.

In the experiment described here, we have studied the momentum and charge distributions of the particles associated with an identified charged particle of large transverse momentum, in proton-proton collisions of c.m.s. energy $\sqrt{s}$ = 52.6 GeV, in the CERN Intersecting Storage Rings (ISR). In what follows we shall call these particles "the associated particles". The large p_T trigger particle was required in a direction close to 90° to the collision axis in the c.m.s. of the colliding protons.

In a previous publication [12] (hereafter referred to as paper I) we have described correlations between the high p_T trigger particle and the forward charged particles in the event. In the present paper we describe correlations between the trigger particle and the associated charged particles in the central region defined by $|y| < 3$, where y is the rapidity.

The paper is organized in the following way: Apparatus, data samples and definition of variables are described in Section 2. Distributions of associated particles in rapidity and azimuth are given in Section 3. Quantum number dependence of the correlation function is discussed in Section 4. Associated momentum in the central region is considered in Section 5. Jet-like structures are described in Section 6. The summary and conclusions are given in Section 7.

2. APPARATUS, DATA SAMPLES, AND DEFINITION OF VARIABLES

2.1 Apparatus

The experiment was carried out at the CERN ISR, using the Split Field Magnet (SFM) and its detector (SFMD) in conjunction with the British-Scandinavian Wide Angle Spectrometer (WAS) which was placed at the SFM in a direction perpendicular to the bisector of the acute angle between the two colliding proton beams.

The main components of the apparatus, WAS, SFM, and SFMD are described in paper I and in references given there. A schematic drawing of the set-up is shown in fig. 1.

The WAS was used to detect and analyse the track of a high p_T particle, and to give a trigger for registration of the event with the SFMD. In order to avoid having the trigger particle traversing the SFMD in an insensitive region around a set of support wires, the WAS was mounted with its axis pointing 4° upwards from the horizontal plane.

2.2 Data samples

The trigger particle in WAS could be unambiguously identified as $\pi^{\pm}$, $K^{\pm}$, p, or $\bar{p}$ in the c.m.s. momentum range 0.5-4.5 GeV/c (see paper I for details). For momenta above 4.5 GeV/c the particle identity could only be classified as "heavy particle" or π.

From the SFMD signals the tracks of about 65% of the charged particles emitted from the pp collisions were found and analysed, giving the charge and momentum vectors at the collision point. This analysis was carried out using the pattern recognition and geometry programs MARC and NICOLE, developed by the CERN Data Handling Division and adapted to this experiment. In the Lorentz transformation to the c.m.s. system a π mass was used for all the associated particles, except for positive particles with $|x| > 0.4$, where a proton mass was used (x is the Feynman variable, $x = 2p_{\ell}^{cms}/\sqrt{s}$).

Table 1 gives the numbers of events, classified according to type and momentum of the trigger particle.

During the experiment a set of events forming an almost unbiased sample of inelastic pp collisions was registered for calibration purposes. It was obtained by using the SFMD in a self-triggering mode, requiring at least two track candidates in the detector. In the analysis it was required that at least two tracks could be reconstructed per event. This trigger was sensitive to $\sim$ 95% of the total inelastic cross-section. The resulting sample (with the elastic events removed) consists of 23,340 events, and is called the minimum bias (MB) sample.

For the major part of the experiment the complete SFMD was available for use in the analysis of the full event, but a part of the experiment was done simultaneously with another experiment [13] which required absorber material placed in the SFM, so that during that time essentially only the very central region was useful for this experiment (see below). In table 1 the events from such "absorber runs" are labelled "A".

2.3 Variables

The events are described in a right-handed Cartesian coordinate system, where the x-axis is pointing radially outwards from the ISR centre, the y-axis is the bisector of the acute angle between the beams, and the z-axis is pointing vertically upwards (see fig. 1). The direction of the trigger particle in WAS is close to the direction of the negative x-axis. In the c.m.s. of the collision the y-axis is along the beams.

$\vec{p} = (p_x, p_y, p_z)$ is the momentum vector of a particle in the c.m.s.

$y = \frac{1}{2} \ln \frac{E + p_y}{E - p_y}$ is the longitudinal rapidity in the c.m.s., where $E = \sqrt{\vec{p}^2 + m^2}$ is calculated with the mass assignment as described above.

$p_T = \sqrt{p_x^2 + p_z^2}$ is the transverse momentum in the c.m.s.

ϕ is the azimuth angle around the beam direction in the c.m.s. $\phi = 0$ in the direction of the positive x-axis (away from the trigger direction). We define $|\phi| \leq 180°$, and we shall refer to the regions $|\phi| > 90°$ and $|\phi| < 90°$ as the TRIGGER side and the AWAY side, respectively.

θ is the polar angle measured from the y-axis in the c.m.s.

p_{TRIG} is the c.m.s. momentum of the trigger particle ($\approx p_T$ of the trigger particle).

2.4 Acceptance

The WAS has a solid angle of $\sim 4 \times 10^{-3}$ sr, with a momentum resolution typically of $\Delta p/p \approx 3\%$ at $p \approx 3$ GeV/c.

In the SFMD the momenta are measured with greatly varying precision, owing to the particular form of the magnetic field and the geometry of the detector. Figure 2 illustrates the average $\Delta p/p$ as a function of the measured momentum for particles in various regions of rapidity and azimuth. It is seen that in particular for particles in the central up-down regions, $|y| < 1$, $60° < |\phi| < 120°$, the momentum is very poorly determined, even below 1 GeV/c. In the remaining regions the momentum resolution varies from a few per cent in the forward region to 10-40% in the central region.

In the above-mentioned absorber runs only associated particles with $|y| < 1$ and $p_T > 0.4$ GeV/c are detected with the same efficiency as for the runs with no absorber material in the SFM.

Figure 3 illustrates the acceptance for particles measured with $\Delta p/p < 0.5$. It is obtained from the particle densities observed in the minimum bias sample and the inclusive single particle spectra [14-18]:

$$\text{Acceptance} = \frac{\text{observed minimum bias density}}{\text{inclusive single particle density}} . \qquad (1)$$

One notices that the acceptance for particles with $p_T > 0.5$ GeV/c in the region $|y| < 1$, $45° < |\phi| < 120°$ is very low. If, however, the requirement $\Delta p/p < 0.5$ is dropped, the acceptance for these particles becomes of the order of 60%.

2.5 The correlation function R

The two-body correlation function for particles 1 and 2 is defined as

$$R = \sigma_{inel} \left\{ \frac{\frac{d\sigma}{dy_1 d\phi_1 dp_{T_1} dy_2 d\phi_2 dp_{T_2}}}{\frac{d\sigma}{dy_1 d\phi_1 dp_{T_1}} \cdot \frac{d\sigma}{dy_2 d\phi_2 dp_{T_2}}} \right\} - 1 \ . \qquad (2)$$

In the present case, particle 1 is the trigger particle, with $y_1 \approx 0$, $\phi_1 \approx 180°$ and $p_{T_1} \approx p_{TRIG}$. The variables with suffix 2 refer to an associated particle. An experimental approximate value of R is found from a sample of N_{TRIG} events, with the trigger particle in a specified parameter range, and a sample of N_{MB} minimum bias events by integrating over suitable parameter regions for the associated particle, i.e.

$$R \approx \frac{\frac{1}{N_{TRIG}} \int \frac{dn_{TRIG}}{dyd\phi dp_T} dyd\phi dp_T}{\frac{1}{N_{MB}} \int \frac{dn_{MB}}{dyd\phi dp_T} dyd\phi dp_T} - 1 \ . \qquad (3)$$

where the suffix 2 has been dropped. dn_{TRIG} and dn_{MB} represent the number of particles found in the element $dy\, d\phi\, dp_T$ at (y,ϕ,p_T) in the triggered and the minimum bias samples, respectively. Both integrations are performed over the same parameter regions, in which the particle densities and the acceptance do not vary too much. Thus the formula simply reduces to

$$R + 1 \approx \frac{\text{mean track density for high } p_T \text{ events}}{\text{mean track density for minimum bias events}} \ . \qquad (4)$$

This representation of the correlation function minimizes the effect of the varying acceptance. It assumes that the acceptance of the SFM detector is the same for the high p_T triggered events as for the minimum bias events, even though the mean multiplicities of observed charged particles in the two cases are 10 and 7, respectively. The corrections to the acceptance due to the different structure of the high p_T triggered events are expected to be small.

With this assumption about the acceptance we find the "true" (acceptance corrected) associated particle densities, ρ, from R and the known [14-18] inclusive single particle densities, ρ_0:

$$\rho = (R + 1)\ \rho_0 \ . \qquad (5)$$

3. DISTRIBUTIONS OF ASSOCIATED PARTICLES IN RAPIDITY AND AZIMUTH

In order to obtain an over-all picture of the distribution of charged particles emitted in events with a high p_T trigger of any type at $\theta = 90°$ we first classify the particles as a low p_T group with $p_T < 0.5$ GeV/c and a high p_T group with $p_T > 0.5$ GeV/c, without restrictions on the precision of the momentum measurement.

$R(y,\phi) + 1$ for the high p_T group obtained with $3.0 < p_{TRIG} < 4.5$ GeV/c is shown in fig. 4, using a cylindrical coordinate system where the coordinates are $R + 1$, ϕ, and the rapidity y.

The main features of fig. 4 are an increase in the value of the correlation function in a small region in y and ϕ near the trigger particle and a much larger increase on the AWAY side, mainly within $|\phi| < 45°$, but extending in rapidity to $|y| \simeq 3$. The events with high p_T triggers are therefore to some degree coplanar.

A clearer picture of this coplanarity is seen when $R + 1$ is plotted as a function of $|\phi|$ for particles in the very central region $|y| < 0.5$, where the increases are largest. This is shown in fig. 5, both for the low p_T and the high p_T group and for two intervals of p_{TRIG}, namely $0.5 < p_{TRIG} < 1.0$ GeV/c and $3.0 < p_{TRIG} < 4.5$ GeV/c.

The main features of fig. 5 are:

i) The correlation function has generally much higher values for the high p_T group than for the low p_T group.

ii) There is a clear dependence on the trigger momentum, with higher values of R for the higher p_{TRIG}, except for a small region around $|\phi| \simeq 125°$, where $R \simeq 0$ for all four distributions.

iii) The distribution for the high p_T group with the high value of p_{TRIG} shows two peaks, one at $\phi = 0°$ and one at $|\phi| = 180°$, both with a half width at half maximum of about 45°.

One may, in particular, note that the value of the correlation function increases with p_{TRIG} also in the up-down regions around $|\phi| = 90°$, with $R \approx 0.5$.

In fig. 6 the correlation function is shown as a function of y in three azimuthal regions, separately for the low p_T and the high p_T group, and for two intervals of the trigger momentum: $0.5 < p_{TRIG} < 1.0$ GeV/c and $3.0 < p_{TRIG} < 4.5$ GeV/c.

A strong increase of R with p_{TRIG} is seen in a broad y-range on the AWAY side ($|\phi| < 30°$). The increase is strongest for the high p_T group. On the TRIGGER side ($|\phi| > 150°$) a strong increase is seen only in the rapidity interval $|y| < 0.5$ and only for the high p_T group. In all three azimuthal regions a negative correlation is seen for large $|y|$, which also becomes more pronounced with increasing p_{TRIG} (see paper I).

4. QUANTUM-NUMBER DEPENDENCE OF THE CORRELATION FUNCTION

We now turn to a discussion of how the correlation function depends on the quantum numbers of the trigger particle and the associated particles. As described above, the trigger particle is identified as π, K, or p, while for the associated particles only the charge is determined. In this section we shall first discuss charge effects by looking at the positive and negative charged particles associated with π^+ and π^- triggers, and then proceed to effects caused by changing the trigger to K or p.

4.1 Charge correlations

Figures 7a and 7b show the y-dependence of R with π^+ triggers, separately for positive and negative associated particles. There are charge effects which are particularly strong on the TRIGGER side for particles with $p_T > 1$ and $|y| < 1$. We therefore select the region $|y| < 1$ and restrict ourselves to $|\phi| < 30°$ on the AWAY side and $|\phi| > 150°$ on the TRIGGER side, where the momentum resolution of the SFMD is sufficiently good to allow a more detailed study of the spectra in terms of the associated particle momentum. Furthermore, when we make comparisons between sets of data for which the SFMD acceptance is identical, we can compare the observed particle densities directly, rather than compare the correlation functions.

Figures 8a and 8b show, as a function of p_{TRIG}, the observed associated particle densities on the TRIGGER side and on the AWAY side. In each case the associated particles are grouped into four p_T intervals, separated according to their charge and trigger type (π^+ or π^-).

On the TRIGGER side (fig. 8a) the following effects are clearly seen:

i) There is a clear charge-compensating effect, in the sense that the density of negative particles associated with π^+ triggers is always higher than that associated with π^- triggers, and conversely for positive particles. This effect becomes more pronounced as p_T increases.

ii) The increase of density with p_{TRIG}, corresponding to the increase of R with p_{TRIG} discussed in Section 3, becomes more pronounced as p_T increases. For $p_T < 0.5$ GeV/c there is little increase with p_{TRIG}, as already indicated in fig. 6. It follows directly that the p_T spectrum of associated particles around the trigger flattens as p_{TRIG} increases.

On the AWAY side (fig. 8b) the situation is quite different:

i) The charge compensating effect is smaller, and it does not change significantly with p_T.

ii) The increase in density with p_{TRIG} is much stronger than on the TRIGGER side, corresponding to the much larger values of R on the AWAY side, discussed in Section 3. Again, the increase with p_{TRIG} becomes stronger as p_T increases, so that the AWAY side p_T spectrum flattens for increasing p_{TRIG}.

The charge compensating effect is seen again in fig. 9, where the quantity

$$R_c = \frac{R^{opposite} + 1}{R^{same} + 1}$$

is shown for π triggers as a function of p_x for the interval $|y| < 1$. $R^{opposite}$ and R^{same} are the correlation functions for particles with the opposite and with the same charge as the trigger particle, respectively.

For all trigger momenta above 1 GeV/c a common dependence on p_x is observed. R_c increases with increasing $|p_x|$ on the TRIGGER side to $R_c \approx 2$ at $p_x = -2$ GeV/c. On the AWAY side ($p_x > 0$), R_c is approximately independent of p_x, with the value $R_c \approx 1.15$. A similar level of the charge-compensating correlation has been observed between the trigger particle and the fast forward particles (see paper I). The fact that R_c has a low value over the whole p_x range for $0 < p_{TRIG} < 1$ GeV/c probably just reflects the similar relationship between large p_{TRIG} and low $|p_x|$, and between low p_{TRIG} and large $|p_x|$.

In order to compare the strengths of the charge-compensating effects for π^+ and π^- triggers, we calculate the charge density $dQ/dyd\phi dp_T$ as the difference between the densities of positive and negative particles, corrected for acceptance [Section 2.5, eq. (5)]. Integrating over p_T and the whole ϕ range we get dQ/dy, which is shown in fig. 10 for π^+ and π^- triggers in the range 2.0-4.5 GeV/c. Also shown is dQ/dy for the single particle inclusive spectrum. It is seen that the charge of a π^- trigger is more strongly compensated within $|y| < 3$ than that of a π^+ trigger. The total associated charge in this y-region for the two trigger types is found to be $Q(\pi^-) = 1.88 \pm 0.09$ and $Q(\pi^+) = 0.44 \pm 0.08$, respectively, while the charge in this region from the inclusive single particle distribution is $Q(\text{incl}) = 0.96$.

4.2 Correlations with other quantum numbers of the trigger particle

We now consider effects also involving other quantum numbers than charge. Figures 11a, b and c show the average particle densities associated with $\pi^\pm$, $K^\pm$, p and $\bar{p}$ trigger particles as functions of p_{TRIG}. The particle densities and the charge correlations associated with different trigger types -- and their increase with p_{TRIG} -- are in general similar, with two exceptions:

i) Events with a p or $\bar{p}$ trigger have about 10% more associated particles with $p_T < 0.5$ GeV/c on the TRIGGER side than events with other types of trigger particles.

ii) It is observed that K^- and $\bar{p}$ triggered events with $p_{TRIG} > 3$ GeV/c have a low content on the AWAY side of negative particles with $p_T > 1.5$ GeV/c as compared to π^- triggered events. The effect is not seen for $p_{TRIG} < 3$ GeV/c.

To study this latter effect further, we show in fig. 12, on a linear scale, the data points from fig. 11c for $p_T > 1.5$ GeV/c and $3.0 < p_{TRIG} < 4.5$ GeV/c. This figure gives a valid basis for comparison of the number of particles with the same charge associated with the different trigger particles, but the ratio between positive and negative associated particles for each trigger type may be influenced by small ($\lesssim 10\%$) acceptance effects. Nevertheless, the data indicate a positive to negative ratio of about 1 for $\pi^\pm$, K^+ and p triggers, and about 2 for K^- and $\bar{p}$ triggers. In order to minimize the effects of the varying acceptance and of the general charge-charge correlations, K^- and $\bar{p}$ triggered events have been normalized to the π^- triggered events, while the K^+ and p triggered events have been normalized to the π^+ triggered events. The results are shown in fig. 13. We conclude that K^- and $\bar{p}$ triggers have a particularly low number of negative associated particles in the considered kinematical region: relative to π^- triggers the numbers are 0.55 ± 0.10 and 0.56 ± 0.16, respectively.

This observation may be connected with the fact that among the six types of trigger particles K^- and $\bar{p}$ are distinguished by not having any valence quarks in common with the incoming protons. This may force specific mechanisms to be dominant at the quark level when a K^- or a $\bar{p}$ trigger is required.

The same effect is shown in fig. 14 in a few rapidity intervals. It is seen that for K^- triggers the effect is strongest in the rapidity interval $0.5 < |y| < 1.0$ (where the number of negative particles relative to that associated with π^- triggers is 0.35 ± 0.13), while for $\bar{p}$ triggers the effect is only significant in the range $|y| < 0.5$ (where the corresponding ratio is found to be 0.32 ± 0.17).

These AWAY side correlations to the type of the trigger particle are not supported by the investigations in the recent FNAL experiment E 494 [19] at a c.m.s. energy $\sqrt{s} = 27.5$ GeV. However, that experiment is concerned with proton-beryllium

collisions and the AWAY side kinematical region which is investigated is a narrow cone around 90° to the collision axis in the proton-nucleon c.m.s., so it is not clear at the present time whether there is a disagreement between the two experiments.

5. ASSOCIATED MOMENTUM IN THE CENTRAL REGION

In this section we shall investigate in more detail the momentum spectrum in the central region, especially for $|y| < 1$. We shall begin by examining the correlation function as a function of p_x of the associated particles, and then consider the associated momentum on the TRIGGER side and the x_E distribution ($x_E = p_x/p_{TRIG}$) on the AWAY side. In the latter two cases we pay particular attention to acceptance corrections and unfold the momentum resolution as described below.

5.1 Dependence of the correlation function on p_x

We have required $\Delta p/p < 0.5$. This cut implies (Section 2.4) that particles with $p_T > 0.5$ GeV/c in the central up-down azimuthal regions are strongly suppressed, but in the same way in the high p_{TRIG} events and in the minimum bias events.

Figures 15a and b show the results obtained for $R(p_x)$ for particles within $|y| < 1$ associated with $\pi^{\pm}$ triggers. Bearing in mind the charge effects discussed in Section 4, we have classified the associated particles according to their charge relative to that of the trigger particle. For both charge combinations the correlation function has a minimum at $p_x \approx -0.3$ GeV/c. This is related to our earlier observation that $R(\phi)$ has a minimum at $|\phi| = 125°$ (see Sections 3 and fig. 5). At the minimum, the value of R is apparently independent of the trigger momentum. The correlation on the TRIGGER side depends strongly on the charge of the associated particle relative to that of the trigger particle.

Although the values of R become quite large at large $|p_x|$, the number of additional particles in this region is in fact quite small. Figure 16 shows the increase of the density of the associated charged particles in three rapidity intervals for $\pi^{\pm}$ triggers when the trigger momentum is increased from

$0.5 < p_{TRIG} < 1.0$ GeV/c to $3.0 < p_{TRIG} < 4.5$ GeV/c. (Acceptance has been corrected for as described in Section 2.5.) One notes that the vast majority of additional particles are at low $|p_x|$, particularly on the AWAY side. In the interval $|y| < 1$, the particle density is seen to increase in two well-defined regions: a weak increase on the TRIGGER side and a much stronger increase on the AWAY side, separated by a small decrease in the region of small negative values of p_x. For the larger $|y|$ values this decrease becomes more pronounced, while the TRIGGER side increase in the particle density disappears. This may be taken as an indication that the observed increase in the particle density near the trigger (for $|y| < 1$) may have a complex composition of an increasing component (e.g. high $|p_x|$ particles following the trigger) and a decreasing one [e.g. a reduction in the number of particles with small negative p_x, due to recoil against the trigger (see also paper I)].

By integration of the spectra in fig. 16 we find the increase in the numbers of associated charged particles per GeV/c increase of p_{TRIG}. This is given in table 2, together with the corresponding increase in the total associated p_x.

On the TRIGGER side we thus find that the positive correlation (which is largely due to particles with charge opposite to the trigger charge) is confined within $|y| < 1$. Summed over the whole $|y| < 3$ range the total increase in the number of particles on the TRIGGER side is negative, and the increase in total p_x is almost zero.

On the AWAY side we find a positive increase both in the number of charged particles and in the total associated p_x for all $|y| < 3$. The fact that in this y region we observe only about half of the additional associated p_x required by transverse momentum balance is presumably due to several factors, e.g. momentum carried by unobserved neutral particles and a recoil of the fast forward particles outside the region $|y| < 3$ (see paper I).

5.2 Corrections to the momentum spectra

The shape of the magnetic field in the SFM makes the momentum resolution in the central region a strongly varying function of direction and momentum, as

already discussed in Section 2.4 (exactly along the x-axis Δp is infinite!). This feature of the SFM makes systematic studies involving varying regions of direction and monentum quite difficult, especially when the momentum is high. The observed spectra will be influenced by the poor momentum measurements in a way which depends on the shape of the true spectra.

Selecting the regions of good pattern recognition efficiency $|\phi| < 25°$ and $|\phi| > 145°$, with $|y| < 1$ in both cases, we treat this problem as follows. At sufficiently high momentum ($p > 400$ MeV/c) multiple scattering is unimportant and the error in the momentum measurement is dominated by the error in a sagitta measurement, leading to a momentum independent value of $\Delta(1/p)$ and a Gaussian distribution in $1/p$ around the true value. This allows us to perform an unfolding of the measured momentum spectra, using an iterative procedure which is found to converge very fast.

The method has been tested on minimum bias events, where the results can be compared with previous measurements of the inclusive spectra [14-18]. It should be noted that these spectra are steeper functions of p_T than the spectra associated with a large p_T trigger particle, and that the corrections are therefore larger. The method used on minimum bias data appears to be reliable up to at least $p_T = 2.5$ GeV/c in the region $|y| < 1$, and since the corrections do not change the momentum spectra by more than 10% when the trigger momentum is large ($p_{TRIG} > > 2$ GeV/c), the main results in this section should be correct within 10%, even when p_T is as large as 4 GeV/c.

A lower pattern recognition efficiency around the trigger track has been corrected for by assuming a smooth variation of the track density near the trigger track.

5.3 Associated momentum on the TRIGGER side

We now go on to investigate the mean value $\langle \sum p_x \rangle$ for the associated charged particles in a specified y and ϕ region. In fig. 17 this quantity for the particles in the interval $|y| < 1$, $|\phi| > 145°$ is shown as a function of p_{TRIG} for

$\pi^{\pm}$, $K^{\pm}$, p, and $\bar{p}$ triggers. The increase in momentum which follows the trigger particle as the trigger momentum is increased is consistent with being linear, with the slopes α indicated on the figure.

In general the values of α are fairly small, with typical values of a few per cent, reaching the highest value of about 5% for $\bar{p}$ triggers. The spectra do not include neutrals, and the effects of using a limited region in y and ϕ are not quite clear. If, however, acceptance corrections are applied in order to include the regions $90° < |\phi| < 145°$ the values of α are changed very little. (This reflects the observation in Section 3 that most of the increase in particle density associated with a large p_T trigger occurs in the region close to the trigger. See also fig. 16.)

To get better statistics in the region where p_{TRIG} is large (larger than 2.5 GeV/c) we also include the data described in Section 2.2, where only the central region is accessible ("absorber runs"). To be sure that there are no systematic problems in adding these two data samples together, some restrictive cuts were made, $|y| < 0.5$, $|\phi| > 145°$ and $|p_x| > 0.4$ GeV/c, and the results from the two sets of data were consistent. The combined result is shown in fig. 18, where it is seen that in this region the spectra associated with the different trigger particle types look more alike than in fig. 17.

It is an interesting question how much of the observed correlations can be explained by the presence of resonances. This is a complicated question, and we plan to return to it in a later publication. The resonances seen by combining the trigger particle with other particles in the event, above a background constructed by combining trigger particles with particles from other events, correspond to approximately 5% of the triggers (fig. 19). The background spectrum has been normalized to the real spectrum in the regions 2.2 to 5.2 GeV/c^2 for π triggers, 2.6 to 5.6 GeV/c^2 for K triggers, and 3.0 to 6.0 GeV/c^2 for p triggers. A preliminary analysis indicates, for example, that $\rho \to \pi^+\pi^-$ can account for 20% of the slope α seen for $\pi^{\pm}$ triggers.

5.4 AWAY side

In order to study further the increase with p_{TRIG} of the particle density on the AWAY side, discussed in Section 3, we restrict the analysis to a region of good acceptance by requiring $|y| < 1$ and $|\phi| < 25°$.

The degree of coplanarity of the high p_T triggered events is illustrated in fig. 20, where we have plotted the particle distribution as a function of $|\phi|$ for two regions of p_T. One sees a marked deviation from an isotropic distribution in ϕ. Also, the ϕ distributions become steeper when p_T is increased.

Another measure of the coplanarity of the events is the steepness of the particle distributions as a function of p_{out}, the momentum component perpendicular to the plane defined by the incoming beam protons and the trigger particle (in our case $p_{out} \approx |p_z|$). The p_{out} distributions shown in fig. 21 are severely limited by the cut $|\phi| < 25°$, necessary due to acceptance. The lines on the figure correspond to an isotropic ϕ distribution. Again, we see a clear deviation from ϕ isotropy.

It is interesting to see whether the AWAY side distribution scales in the variable $x_E = p_x/p_{TRIG}$, as expected in some hard-scattering models. On fig. 22 the quantity $(1/N_{TRIG})(dn/dx_E)$ is shown as a function of p_{TRIG} for fixed intervals of x_E, including only particles with $p_{out} < 0.5$ GeV/c. One sees a strong indication of scaling for $p_{TRIG} > 3$ GeV/c.

To investigate whether the presence in these high p_T events of particles not directly related to the high p_T process can explain the approach from <u>above</u> to a scaling curve, we have calculated the contribution from such a source, assuming that these "background particles" behave as in minimum bias events. As seen on the graph the subtraction of such a background diminishes the deviation from scaling, although it does not change the results very much.

The x_E distribution has also been investigated for the six different trigger particle types, but no significant differences were found.

In fig. 23a the x_E distribution is shown for $p_{TRIG} > 3$ GeV/c in several intervals of p_{TRIG}. The spectrum is approximately exponentially decreasing in x_E. In order to compare the slope with that obtained in the study of e^+e^- collisions a better variable to use would be

$$x_E' = \frac{p_x}{\left(1 + \frac{3}{2}\alpha\right)p_{TRIG}} = \frac{x_E}{1 + \frac{3}{2}\alpha},$$

where we have included the momentum of the particles which follow the trigger particle (α is the slope parameter described in Section 5.3). The factor $^3/_2$ is used in order to include the momentum of unobserved neutral particles, and the values for α are taken from fig. 24, where α is seen to vary as a function of x_E approximately as $\alpha = 0.015 + 0.1\, x_E$. The resulting contribution is shown in fig. 23b, where we have grouped the whole interval $3 < p_{TRIG} < 6$ GeV/c together. The straight line on the figure, which represents an exponential fit to our data, has a slope of -9.0 ± 0.2. The shape of this distribution is close to the shapes observed for the corresponding distributions in other proton-proton experiments, both at the ISR [1-3] and FNAL [4]. The distribution is also similar to, although somewhat steeper than, the distributions found in e^+e^- collisions at SLAC [20] and at DESY [21,22].

Finally, we note that there is a complicated interplay between the structure on the TRIGGER side and on the AWAY side. Figure 24 shows, as an example, the momentum following the trigger particle as a function of p_{TRIG}, for five different intervals of the largest x_E found on the AWAY side. It is seen that the presence of particles on the AWAY side and the magnitude of their momenta substantially changes the value of the slope α of the accompanying momentum on the TRIGGER side.

6. JET-LIKE STRUCTURE

In this section, we investigate to what extent our results show evidence for jet-like structures similar to those already observed in other experiments.

The observed growth of the particle density over a broad range of rapidity ($|y| < 3$) on the AWAY side when p_{TRIG} is increased (fig. 6) has already been discussed. In order to study further the structure of this broad distribution of particles, we investigate the distribution in the rapidity difference Δy between any two AWAY side high p_T particles observed in an event. The result is shown in fig. 25 for pairs of particles with $p_T > 0.8$ GeV/c associated with triggers with $2.5 < p_{TRIG} < 6.0$ GeV/c. The particles were required to be within $|\phi| < 30°$ and to have $\Delta p/p < 0.5$. The character of the results is not sensitive to the precise values of the p_{TRIG} and the p_T cuts.

We have also constructed a sample of particle pairs by combining one particle from one event with one particle from another, subject to the same cuts as those described above. The pairs formed by particles from the same event have a Δy distribution with a strong peak within $\Delta y < 1$, as compared to the corresponding distribution for the pairs formed by particles from different events, also shown on fig. 25. The shapes of the two distributions are very similar for $\Delta y > 1$. It is therefore natural to take the "mixed events distribution" as a representation of a background to a correlation phenomenon, an "AWAY side jet". Figure 26 shows the difference between the two Δy distributions, normalized to the same area for $\Delta y > 1$. The correlation peak seen in the region of small Δy is the primary evidence for an AWAY side jet in the present experiment. The peak has a half width at half maximum of $\Delta y = 0.5$, and it is a factor of two larger for pairs of oppositely charged particles than for pairs of particles with the same charge.

The cut $|\phi| < 30°$ is necessary due to the variation of the acceptance with ϕ, and with this rather limited ϕ region a study of the $\Delta\phi$ distribution similar to that of the Δy distribution discussed above cannot be done. The particles are correlated in ϕ to the fixed direction of the trigger particle, with a distribution which is fairly broad compared with the acceptance region (fig. 5). In order to see a $\Delta\phi$ correlation we need high statistical accuracy, and we have found it necessary to include the "absorber data" at the cost of restricting the y region to $|y| < 1$. Furthermore, we have chosen pairs of oppositely charged particles in the

peak region $\Delta y < 0.6$ of Fig. 25. For these points the observed $\Delta\phi$ distribution and the "background" curve constructed from mixed events (normalized to the same area) are shown in fig. 27. It is seen that although the "background" curve describes the $\Delta\phi$ distribution to some extent, there is a difference in shape, as expected.

We conclude from these observations that in a few per cent of the events two or more high p_T charged particles are observed close together in rapidity on the AWAY side. The rapidity of this group of particles (considered as <u>one</u> system) changes from event to event, with a broad distribution ranging over about ±3 units.

Having seen indications of jet-like structures on the AWAY side, we shall now proceed to study the q distribution for particles within such a "jet". q is the momentum component transverse to the "jet axis", which is defined to be parallel to the total momentum vector of the jet. Again, we restrict our study to the simple case of pairs of charged high p_T particles, and regard the direction of the total momentum of the pair as an approximation to the direction of the jet axis (a more comprehensive study of jet-like systems will appear in a forthcoming paper).

We consider pairs of AWAY side particles with $p_T > 0.8$ GeV/c. If no other selection criteria were applied, the q distribution would be strongly influenced by the acceptance function and the p_T cut. Therefore, we only accept particles within $|y| < 1$ and $|\phi| < 30°$, where the acceptance is reasonably uniform. The jet system is then required to be very central: $|y_{jet}| < 0.2$ and $|\phi_{jet}| < 10°$ (where y_{jet} and ϕ_{jet} are the rapidity and azimuth angle, respectively, for the <u>pair</u> of particles), and the plane of the two particles is required to be inclined less than 30° with respect to the plane defined by the beams and the jet axis. Finally, in order to avoid the bias introduced by the p_T cut, we require each particle in the pair to have a longitudinal momentum along the jet axis larger than 1 GeV/c.

With this set of selection criteria the q distribution is unbiased by the acceptance for $0.1 < q < 0.8$ GeV/c. The result is shown in fig. 28 for events with $p_{TRIG} > 1$ GeV/c. The figure also shows the estimated "background" distribution

again constructed from a "mixed events" sample, applying the same cuts as described above. The normalization of the "background" is determined from the observed rate of particles with $p_T > 0.8$ GeV/c extrapolated to $p_{TRIG} = 0$, with the assumption that this "background" rate is independent of p_{TRIG}.

The q distribution after subtraction of the background is also shown on fig. 28. Over the unbiased q range ($q < 0.8$ GeV/c) this distribution is well described by an exponential:

$$\frac{1}{q}\frac{dN}{dq} = A\, e^{-Bq} , \qquad (6)$$

with $B = 2.5 \pm 0.7$ $(GeV/c)^{-1}$. This corresponds to an average value $\langle q \rangle = 0.80 \pm$ $\pm$ 0.25 GeV/c. Particles of lower p_T have a much steeper q distribution relative to the "jet axis" defined by the pair of high p_T ($p_T > 0.8$ GeV/c) particles, but since estimates show that the low p_T region is dominated by particles from the "background event", and since we have no simple way of distinguishing between "jet particles" and "background particles", we have not investigated the properties of "jet particles" of low momenta.

Turning now to the TRIGGER side, we have already noted (figs. 5 and 6) that with increasing p_{TRIG} there is an increasing probability of finding associated high p_T particles close to the trigger particle in rapidity and azimuth. The total number of additional particles, as well as the additional momentum, is quite small, 0.022 ± 0.007 particles and 31 ± 4 MeV/c, respectively, per GeV/c increase of p_{TRIG} (table 2).

Using the events where a large p_T charged particle is observed close to the trigger, we can obtain a relatively unbiased q distribution for particles in a "TRIGGER side jet" in a similar way as for the "AWAY side jet". We choose events with $p_{TRIG} > 2.5$ GeV/c and require the associated particle to have $p_T > 1$ GeV/c and $|y| < 1$. The plane defined by the trigger particle and the associated particle is again required to be inclined less than 30° with respect to the beam-trigger plane. In this case the background is estimated by imposing a typical trigger

spectrum with $p_{TRIG} > 2.5$ GeV/c on a sample of minimum bias events, assuming that "background particles" are similar to minimum bias particles in rate and distribution. The resulting q distributions are shown in fig. 29. Again, the subtracted distribution is well described in the unbiased q range by the exponential given in eq. (6). In this case we find $B = 3.8 \pm 0.3$ $(GeV/c)^{-1}$, which corresponds to an average value $\langle q \rangle = 0.52 \pm 0.05$ GeV/c.

It should be noted that the kinematical configurations represented by these pairs of particles are probably not typical for "jet particles", in particular in that the longitudinal momentum along the "jet axis" is fairly large. The difference in the observed values of $\langle q \rangle$ on the TRIGGER side and on the AWAY side is quite possibly due to the difference in the selection criteria for "jets" on the two sides.

Another quantity of interest is the mean value of z, the fraction of the "TRIGGER side jet" momentum carried by the trigger particle. If we assume that $\langle \sum p_x \rangle$, the mean momentum following the trigger particle, is a linear function of p_{TRIG} with slope α (Section 5), we can write $\langle z \rangle = (1 + \alpha)^{-1}$. The values for α given on fig. 18 and in table 2 give $\langle z \rangle \approx 0.97$. We emphasize that this result does not include effects of the momentum carried by neutral particles, y and ϕ cuts, and, in particular, possible dependence of $\langle z \rangle$ on jet momentum.

The general observations in this section show that the charged particle distributions in high p_T triggered events are consistent with a picture [5-11], where these events are basically originating from hard scattering processes between constituents of the incoming protons, and where the TRIGGER side and the AWAY side jets are the fragmentation products of the two scattered constituents, the TRIGGER side jet being severely biased through the trigger requirement of one high p_T particle [8,11]. With the rest system of the colliding constituents having predominantly longitudinal motion in the pp c.m.s., the two jets should tend to be coplanar, but not collinear, in accordance with the observations.

7. SUMMARY AND CONCLUSIONS

We have studied a sample of proton-proton collisions at $\sqrt{s}$ = 52.6 GeV, from which a charged, identified hadron (the trigger particle) is emitted close to 90° to the beams in the c.m.s. with a transverse momentum in the range 0.5-4.5 GeV/c (0.5-6.0 GeV/c for $\pi^{\pm}$ triggers).

In the present paper we have presented results on the charged-particle distribution in the central region associated with the trigger particle.

The main results are:

i) The charged particles associated with a high p_T trigger particle are concentrated in the azimuthal regions close to the trigger plane, with a distribution having a half width at half maximum of $\sim 45°$.

ii) There is a strong charge-compensating correlation between the trigger particle and the associated particles with $|y| < 1$ on the TRIGGER side. Outside this region a charge-compensating correlation to the trigger is present at a level of about 15%.

iii) Apart from the above-mentioned charge effects, the distribution of the charged particles is not very sensitive to the type of the trigger particle. However, at least 5% of the trigger particles are seen to come from resonances. For K^- triggers with momentum above 3 GeV/c, the AWAY side region $|y| < 1$, $p_T > 1.5$ GeV/c, contains only about half as many negative particles per event as for other trigger particles, while the number of positive particles is approximately the same. A similar, but statistically less significant, effect is seen for $\bar{p}$ triggers.

iv) There is a positive correlation between the trigger particle and the associated particles in almost all of phase space. The correlation is particularly strong for associated particles on the AWAY side within the region $|y| < 3$, $|\phi| < 45°$, and within a smaller region $|y| < 1$, $|\phi| > 135°$ on the TRIGGER side. The correlation increases strongly in both of these regions with increasing momentum of the trigger particle, most for associated particles of high p_T.

Owing to the steep decrease of the inclusive cross-section with increasing p_T, the increase in the associated particle density itself is largest for particles of low p_T on the AWAY side and for particles with p_T near 1 GeV/c on the TRIGGER side. For each GeV/c increase of the trigger momentum, the total increase in the number of associated charged particles per event in the y and ϕ regions mentioned above is 0.8 particles on the AWAY side and 0.02 particles (predominantly of charge opposite to that of the trigger particle) on the TRIGGER side. Similarly, the increase of the charged particle momentum in the same regions is 0.5 GeV/c on the AWAY side and 35 MeV/c on the TRIGGER side, per GeV/c increase of p_{TRIG}.

v) The AWAY side particle distribution within $|y| < 1$ and $p_{out} < 0.5$ GeV/c as a function of the parameter $x_E = p_x/p_{TRIG}$ changes with the trigger momentum up to $p_{TRIG} \approx 3$ GeV/c. For $p_{TRIG} > 3$ GeV/c and $x_E > 0.3$ it appears to be independent of p_{TRIG}.

vi) On the AWAY side there is a positive two-particle correlation between high p_T associated particles with a width of about $\Delta y \approx 0.5$. Particles with opposite charges are more strongly correlated than particles with the same charge. Operationally defining a "jet" as a pair of high p_T ($p_T > 0.8$ GeV/c) particles we find that the rapidity of the AWAY side jet changes from event to event with a distribution ranging over about ±3 rapidity units. The distribution $(1/q)/(dN/dq)$ for particles within such pairs (after some additional cuts), where q is the momentum transverse to the jet axis (defined by the direction of the total momentum vector of the pair), shows an exponentially decreasing behaviour for small values of q. The average value $\langle q \rangle$ for this exponential distribution is found to be 0.80 ± 0.25 GeV/c for such AWAY side jets and 0.52 ± 0.05 GeV/c for TRIGGER side jets (pairs consisting of the trigger particle and an associated high p_T TRIGGER side particle).

Current theoretical models for high p_T hadronic collisions are concerned with the nature of the colliding constituents and of the objects emerging from the hard scattering process. Several specific mechanisms are under discussion:

$qq \rightarrow qq$ quark-quark scattering

$Mq \rightarrow Mq$ meson-quark scattering

$q\bar{q} \rightarrow MM$ quark-antiquark fusion

$qg \rightarrow qg$ quark-gluon scattering

$gg \rightarrow gg$ gluon-gluon scattering

Our observation that the trigger particle is usually unaccompanied by other particles close to it in rapidity and azimuth is most easily reconciled, within this framework, with models which produce a meson in the final state, e.g. the meson-quark scattering (Constituent Interchange Model) [9] or the quark fusion [8,11] mechanisms. The high ratio of positive to negative particles opposite a K^- or $\bar{p}$ trigger also finds a natural explanation in these models. Thus our results seem to indicate important contributions from these mechanisms to high p_T processes in the studied p_T range. All the different basic processes enter however in a comprehensive theory like QCD, and this may well be in accordance with the observations.

Acknowledgements

It is a pleasure to thank the SFM detector group and the staff of the ISR Division at CERN for their help, and members of the CERN programming staff for their assistance in the on-line and off-line analysis. We would also like to thank Ph. Dam, B. Guillerminet, P. Herbsleb, J.E. Hooper, D. Korder, E. Lohse, D.B. Smith and M.-I. Sundell for their contribution and assistance. Some authors (S.A., X. de B., H.B.J., A.K., B.L., H.E.M., R.M., and P.V.) acknowledge financial support from CERN during part of the experiment.

We gratefully acknowledge support from the CERN and Rutherford computing facilities and from the computer centres at Bergen, Copenhagen and Lund Universities. We also acknowledge the loan of electronics from the Laboratory for Nuclear Science of the Massachusetts Institute of Technology.

The experiment was supported by the United Kingdom Science Research Council, The Danish and Swedish Natural Science Research Councils, The Norwegian Research

Council for Science and the Humanities, and L'Institut National de Physique Nucleaire et de Physique des Particules, France.

REFERENCES

[1] P. Darriulat, P. Dittmann, K. Eggert, M. Holder, K.T. McDonald, T. Modis, F.L. Navarria, A. Seiden, J. Strauss, G. Vesztergombi and E.G.H. Williams, Nuclear Phys. B107 (1976) 429.

[2] M. Della Negra, D. Drijard, H.G. Fischer, G. Fontaine, H. Frehse, P. Frenkiel, C. Ghesquière, R. Gokieli, P. Hanke, W. Hofmann, P.G. Innocenti, W. Isenbeck, E.E. Kluge, V. Korbel, D. Linglin, A. Minten, A. Norton, A. Putzer, G. Sajot, R. Sosnowski, S. Stein, J. Stiewe, H.D. Wahl and D. Wegener, Nuclear Phys. B127 (1977) 1.

[3] M. Della Negra, D. Drijard, H.G. Fischer, G. Fontaine, H. Frehse, P. Frenkiel, G. Ghesquière, R. Gokieli, P. Hanke, P.G. Innocenti, W. Isenbeck, E.E. Kluge, V. Korbel, S. Krzywdzinski, D. Linglin, A. Minten, D.R.O. Morrison, A. Putzer, H. Schneider, R. Stroynowski, S. Stein, W.J. Schwille and D. Wegener, Phys. Letters 59B (1975) 401.

[4] C. Bromberg, G. Fox, R. Gomez, J. Pine, S. Stampke, K. Yung, S. Erhan, E. Lorenz, M. Medinnis, J. Rohlf, P. Schlein, V. Ashford, H. Haggerty, R. Juhala, E. Malamud, S. Mori, R. Abrams, R. Delzenero, H. Goldberg, S. Margulies, D. McLeod, J. Solomon, R. Stanek, A. Dzierba and W. Kropac, Phys. Rev. Letters 38 (1977) 1447 and Fermilab-Conf-77/62-Exp.

[5] R.D. Field and R.P. Feynman, Phys. REv. D 15 (1977) 2590.

[6] R.P. Feynman, R.D. Field and G.C. Fox, Nuclear Phys. B128 (1977) 1.

[7] R.P. Feynman, R.D. Field and G.C. Fox, Caltech preprint, Calt-68-651, May 1978.

[8] S.D. Ellis, M. Jacob and P.V. Landshoff, Nuclear Phys. B108 (1976) 93. M. Jacob and P.V. Landshoff, Nuclear Phys. B113 (1970) 395.

[9] R. Blankenbecler, S.J. Brodsky and J.F. Gunion, Phys. Letters 39B (1972) 649.

[10] P.V. Landshoff and J.C. Polkinghorne, Phys. Rev. D 8 (1973) 4157.

[11] P.V. Landshoff, Review talk at the Workshop on Future ISR Physics, CERN, Sept. 1977, Document ISR Workshop/2-7, Oct. 1977, edited by M. Jacob.

[12] M.G. Albrow, S. Almehed, P.S.L. Booth, X. de Bouard, H. Bøggild, L.J. Carroll, P. Catz, E. Dahl-Jensen, I. Dahl-Jensen, G. Damgaard, G. von Dardel, M. Davidson, N. Elverhaug, B. Guillerminet, K.H. Hansen, P. Herbsleb, J.E. Hooper, J.N. Jackson, G. Jancso, G. Jarlskog, H.B. Jensen, L. Jönsson, A. Klovning, E. Lillethun, E. Lohse, A. Lu, B. Lörstad, N.A. McCubbin, H.E. Miettinen, J.V. Morris, R. Møller, S.Ø. Nielsen, J.O. Petersen, J.A.J. Skard, D.B. Smith and P. Villeneuve, Nuclear Phys. B135 (1978) 461.

[13] Experiment R414, CERN-Heidelberg-Hamburg-Orsay-Vienna Collaboration.

[14] B. Alper, H. Bøggild, P. Booth, F. Bulos, L.J. Carroll, G. Damgaard, G. von Dardel, B. Duff, K.H. Hansen, F. Heymann, J.N. Jackson, G. Jarlskog, L. Jönsson, A. Klovning, L. Leistam, E. Lillethun, E. Lohse, G. Lynch, G. Manning, K. Potter, M. Prentice, P. Sharp, S. Sharrock, S. Ølgaard-Nielsen, D. Quarrie and J.M. Weiss, Nuclear Phys. B100 (1975) 237.

[15] P. Capiluppi, G. Giacomelli, A.M. Rossi, G. Vannini, A. Bertin, A. Bussiére and R.J. Ellis, Nuclear Phys. B79 (1974) 189.

[16] A.M. Rossi, G. Vannini, A. Bussiére, E. Albini, D. D'Alessandro and G. Giacomelli, Nuclear Phys. B84 (1975) 269.

[17] M.G. Albrow, A. Bagchus, D.P. Barber, A. Bogaerts, B. Bosnjakovic, J.R. Brooks, A.B. Clegg, F.C. Erné, C.N.P. Gee, D.H. Locke, F.K. Loebinger, P.G. Murphy, A. Rudge, J.C. Sens and F. van der Veen, Nuclear Phys. B56 (1973) 333 and Nuclear Phys. B73 (1974) 40.

[18] D. Antreasyan, J.W. Cronin, H.J. Frisch, M.J. Schocket, L. Kluberg, P.A. Piroué and R.L. Sumner, Phys. Rev. Letters 38 (1977) 112 and 115.

[19] R.J. Fisk, R.J. Engelmann, M.L. Good, A.S. Ito, H. Jöstlein, D.M. Kaplan, R.D. Kephart, R.L. McCarthy, H. Wahl, S.W. Herb, D.C. Hom, L.M. Lederman, J.C. Sens, H.D. Snyder, J.K. Yoh, J.A. Appel, B.C. Brown, C.N. Brown, W.R. Innes and K. Ueno, Phys. Rev. Letters 40 (1978) 984.

[20] G. Hanson, Talk given at the XVIIIth Internat. Conf. on High-Energy Physics, Tbilisi, USSR, 1976; SLAC-PUB-1814 (1976).

[21] R. Brandelik. W. Braunschweig, H.-U. Martyn, H.G. Sander, D. Schmitz, W. Sturm, W. Wallraff, D. Cords, R. Felst, R. Fries, E. Gadermann, H. Hultschig, P. Joos, W. Koch, U. Kötz, H. Krehbiel, D. Kreinick, W.A. McNeely, K.C. Moffeit, O. Römer, R. Rüsch, B.H. Wiik, G. Wolf, G. Grindhammer, J. Ludwig, K.H. Mess, A. Petersen, G. Poelz, J. Ringel, K. Sauerberg, P. Schmüser, W. De Boer, G. Buschhorn, B. Gunderson, R. Kotthaus, H. Lierl, H. Oberlack, M. Schliwa, S. Orito, T. Suda, Y. Totsuka and S. Yamada, Phys. Letters 67B (1977) 358.

[22] G. Knies, Proc. Internat. Symposium on Lepton and Photon Interactions at High Energies, Hamburg, 1977 (DESY, Hamburg, 1977), p. 93.

Table 1

Trigger spectrum of the studied sample

p_{TRIG} (GeV/c)		π^+	π^-	K^+	K^-	p	$\bar{p}$	K^+/p	$K^-/\bar{p}$
0.5-1.0		3023	1923	1993	1213	1406	2344	-	-
1.0-2.0		13399	9150	4154	2765	6515	4540	-	-
2.0-2.5		3749	3107	435	203	378	134	-	-
2.5-3.0		4197	3531	1312	775	1189	389	-	-
	A	4495	4334	1658	1129	1479	539	-	-
3.0-4.5		2569	2044	1019	558	601	177	26	13
	A	3185	2862	1404	832	880	313	43	16
4.5-6.0		129	93	-	-	-	-	61	18
	A	152	127	-	-	-	-	62	26
0.5-6.0		34951	27277	11984	7490	12451	8443	192	91
3.0-6.0		6035	5126	2423	1390	1481	490	192	91
Minimum Bias sample (elastic events removed): 23340									

The letter A refers to the "absorber data" (see text)

Table 2

The increase per event of the mean number of associated particles, $\langle n \rangle$, and of the mean sum of their x-component of momentum, $\langle \Sigma p_x \rangle$, per GeV/c increase in the mean trigger momentum. The asterisk indicates values obtained when only associated particles of opposite charge to that of the trigger particle were considered.

	$\frac{\Delta\langle n \rangle}{\Delta\langle p_{TRIG} \rangle} \times 10^3$ $(GeV/c)^{-1}$		$\frac{\Delta\lvert\langle \sum p_x \rangle\rvert}{\Delta\langle p_{TRIG} \rangle} \times 10^3$	
y range	TRIGGER side	AWAY side	TRIGGER side	AWAY side
$\lvert y \rvert < 1$	-22 ± 7	510 ± 30	31 ± 4	287 ± 34
$1 < \lvert y \rvert < 2$	-29 ± 18	250 ± 20	-5 ± 4	160 ± 10
$2 < \lvert y \rvert < 3$	-69 ± 15	80 ± 20	-23 ± 4	56 ± 10
$\lvert y \rvert < 3$	-76 ± 20	840 ± 40	3 ± 7	503 ± 37
$\lvert y \rvert < 1^*$	24 ± 4	260 ± 20	28 ± 4	143 ± 21

Figure captions

Fig. 1 : Schematic plan view of the apparatus. The beams intersect in the vacuum chamber inside the Split Field Magnet (SFM). In the Wide Angle Spectrometer (WAS) BM is a bending magnet, SC1-SC5 are spark chambers, 1H-4H and 2V-4V are horizontal and vertical scintillator hodoscopes, respectively, and $\check{C}1$-$\check{C}2$ are gas Čerenkov counters. The coordinate system used is also shown.

Fig. 2 : Curves representing the average momentum resolution $\langle \Delta p/p \rangle$ for SFMD tracks, as a function of the measured value of the momentum for particles in various regions of c.m.s. rapidity and in the azimuth intervals $60° < |\phi| < 120°$ (dashed line) and $|\phi| < 30°$ or $|\phi| > 150°$ (full line).

Fig. 3 : Acceptance functions for charged particles with $p_T < 0.5$ GeV/c (full line) and $p_T > 0.5$ GeV/c (dashed line), when $\Delta p/p < 0.5$ is required.

Fig. 4 : The average distribution of charged particles with $p_T < 0.5$ GeV/c in high p_T events ($\langle p_{TRIG} \rangle \approx 3.4$ GeV/c) relative to the distribution observed in minimum bias events. The ratio R + 1 is shown as a function of y and ϕ in cylindrical coordinates. The coordinate system (R + 1, ϕ, y) is indicated in the insert.

Fig. 5 : R + 1 as a function of ϕ in the rapidity range $|y| < 0.5$ for two intervals of p_{TRIG} and for a) $p_T < 0.5$ GeV/c, b) $p_T > 0.5$ GeV/c.

Fig. 6 : The rapidity dependence of R + 1 in the three azimuthal regions: the TRIGGER side, $|\phi| > 150°$; the up-down regions, $60° < |\phi| < 120°$; and the AWAY side, $|\phi| < 30°$ for a) charged particles with $p_T <$ < 0.5 GeV/c and b) charged particles with $p_T > 0.5$ GeV/c. In both cases R(y) + 1 is given for two intervals of p_{TRIG}.

Fig. 7 : a) The correlation function R + 1 for π^+ trigger particles and associated charged particles with $|\phi| > 150°$ on the TRIGGER side, as a function of rapidity and charge of the associated particle for two regions of p_T and four intervals of p_{TRIG}.

b) As (a), but for associated charged particles within $|\phi| < 30°$ on the AWAY side.

Fig. 8 : a) The average number of observed charged particles per event on the TRIGGER side within $|y| < 1$, $|\phi| > 150°$ associated with π^+ and π^- trigger particles, shown as a function of p_{TRIG} for different values of p_T (in GeV/c).

b) As (a), but for associated charged particles on the AWAY side within $|\phi| < 30°$.

Fig. 9 : The correlation between the charge of the trigger particle ($\pi^{\pm}$) and the charge of the associated charged particles within $|y| < 1$, as measured by the ratio

$$R_c = \frac{R^{\text{opposite charge}} + 1}{R^{\text{same charge}} + 1}$$

as a function of p_x for four intervals of p_{TRIG}.

Fig. 10 : The average charge per unit of rapidity of particles associated with π^- and π^+ trigger particles, respectively. The corresponding quantity for the inclusive spectrum is also indicated.

Fig. 11 : The average number of observed associated particles per event on the TRIGGER side within $|y| < 1$, $|\phi| > 150°$, with the six different types of trigger particles, as functions of p_{TRIG} and p_T (in GeV/c). The number of associated particles with a) the same charge as that of the trigger particle and b) the opposite charge are shown separately; c) The average number of observed associated particles per event on the AWAY side within $|y| < 1$, $|\phi| < 30°$, with the six different types of trigger particles, as functions of p_{TRIG} and p_T (in GeV/c).

Fig. 12 : The average number of observed positive and negative particles with $p_T > 1.5$ GeV/c on the AWAY side within $|y| < 1$, associated with the six different types of trigger particles with $3.0 < p_{TRIG} < 4.5$ GeV/c.

Fig. 13 : The observed densities of AWAY side positive and negative particles with $p_T > 1.5$ GeV/c and $|y| < 1$ associated with K^- and $\bar{p}$ triggers relative to the observed densities associated with π^- triggers, and the corresponding densities associated with K^+ and p triggers relative to the densities associated with π^+ triggers for $3.0 < p_{TRIG} < 4.5$ GeV/c.

Fig. 14 : The densities of positive and negative AWAY side particles with $p_T > 1.5$ GeV/c within $|\phi| < 30°$ associated with K^- and $\bar{p}$ triggers, relative to the corresponding densities associated with π^- triggers as functions of rapidity for $3.0 < p_{TRIG} < 4.5$ GeV/c.

Fig. 15 : The correlation function R as a function of p_x and p_{TRIG} for particles within $|y| < 1$ associated with $\pi^\pm$ trigger particles, separately for associated particles with a) the opposite charge of that of the trigger particle and b) the same charge.

Fig. 16 : The increase in the density of charged particles associated with $\pi^\pm$ trigger particles when the trigger momentum is increased from $0.5 < p_{TRIG} < 1.0$ GeV/c ($\langle p_{TRIG} \rangle = 0.8$ GeV/c) to $3.0 < p_{TRIG} < 4.5$ GeV/c ($\langle p_{TRIG} \rangle = 3.4$ GeV/c). The particle density increase is shown as a function of p_x for three different intervals of $|y|$.

Fig. 17 : The mean value per event of the sum of the momentum component p_x of associated particles within $|y| < 1$ and $|\phi| > 145°$ (TRIGGER side) as a function of the trigger momentum for $\pi^\pm$, $K^\pm$, p and $\bar{p}$ triggers. The slopes $\alpha = d\langle|\sum p_x|\rangle/dp_{TRIG}$ obtained by linear least squares fits are indicated.

Fig. 18 : As fig. 17, but for $|y| < 0.5$ and with the additional requirement that $p_x > 0.4$ GeV/c. Here the "absorber run" sample described in the text is included.

Fig. 19 : The two-particle mass distributions of the systems of a trigger particle combined with other particles observed in the SFMD and assumed to be pions. A background spectrum, constructed as described in the text, has been subtracted.

Fig. 20 : The ϕ distribution of charged particles on the AWAY side for $|y| < 1$ in two intervals of p_T when $p_{TRIG} > 2.5$ GeV/c, compared with the minimum bias level multiplied by the indicated factors. The lines represent Gaussian fits to the data points with $\sigma_\phi = 30°$ for $0.5 < p_T < 1.0$ GeV/c and $\sigma_\phi = 26°$ for $p_T > 1.0$ GeV/c.

Fig. 21 : The distribution of p_{out}, $(1/N_{TRIG})(dn/dp_{out})$ in intervals of p_x for particles with $|y| < 1$ and for $p_{TRIG} > 2.5$ GeV/c. The histogram lines correspond to the distribution one would obtain if the AWAY side p_T distribution for $|\phi| < 25°$ were independent of ϕ.

Fig. 22 : The value of $(1/N_{TRIG})(dn/dx_E)$ in intervals of x_E for particles on the AWAY side with $|y| < 1$ and $p_{out} < 0.5$ GeV/c, as a function of p_{TRIG}. The crosses represent the result after subtracting a background estimate as described in the text.

Fig. 23 : a) $(1/N_{TRIG})(dn/dx_E)$ for AWAY side particles with $|y| < 1$ and $p_{out} < 0.5$ GeV/c as a function of x_E in four intervals of the trigger momentum (indicated in GeV/c on the figure).

b) The distribution $(1/N_{TRIG})(dn/dx'_E)$ (see text for the definition of x'_E) for AWAY side particles with $|y| < 1$ and $p_{out} < 0.5$ GeV/c when $3.0 < p_{TRIG} < 6.0$ GeV/c. The line represents an exponential fit to the points, giving a slope of -9.0 ± 0.2.

Fig. 24 : The mean value per event of the sum of the momentum component p_x of associated particles with $p_x > 0.4$ GeV/c within $|y| < 0.5$ and $|\phi| > 145°$ (TRIGGER side) as a function of p_{TRIG} for π triggers. The events have been divided into four groups according to the value of the largest x_E observed within $|y| < 1$, $|\phi| < 25°$ on the AWAY

Fig. 29 : The distribution $(1/N_{TRIG})(1/q)(dn/dq)$ on the TRIGGER side for pairs of particles of which one is a trigger particle with $p_{TRIG} > 2.5$ GeV/c and the other a charged particle with $p_T > 1$ GeV/c, $|\phi| > 145°$, and $|y| < 1$. The background has been estimated as described in the text, and the difference between the real spectrum and the estimated background is also shown.

side, and one group for the events where no charged particles were observed in this region on the AWAY side. The slope α is indicated on the figure for each group. The data from the "absorber runs" have been included.

Fig. 25 : The distribution of the difference in rapidity ($\Delta y = |y_1 - y_2|$) for pairs of particles on the AWAY side with $p_T > 0.8$ GeV/c and $|\phi| < 30°$, when $2.5 < p_{TRIG} < 6.0$ GeV/c. The distribution is shown separately for neutral and doubly charged pairs. The histograms represent the uncorrelated distributions, obtained as described in the text.

Fig. 26 : As fig. 25, with the uncorrelated distributions normalized for $\Delta y > 1$ and subtracted as background.

Fig. 27 : The distribution of the difference in ϕ for pairs of oppositely charged particles on the AWAY side with $p_T > 0.8$ GeV/c and $|\phi| < 30°$ for $2.5 < p_{TRIG} < 6.0$ GeV/c. These pairs are selected such that Δy is in the peak region of fig. 25 ($\Delta y < 0.6$). The curve represents the uncorrelated background constructed from mixed events and normalized to the same area as the real distribution.

Fig. 28 : The distribution $(1/N_{TRIG})(1/q)(dn/dq)$ for pairs of particles on the AWAY side with $p_T > 0.8$, $|y| < 1$ and $|\phi| < 30°$, when $p_{TRIG} > 1$ GeV/c. Additional cuts, described in the text, have been imposed to obtain an unbiased q distribution in the range $0.1 < q < 0.8$ GeV/c. A background distribution has been constructed by combining particles from different events and applying the same cuts. The normalization of the background is described in the text. The difference between the real spectrum and the estimated background is also shown.

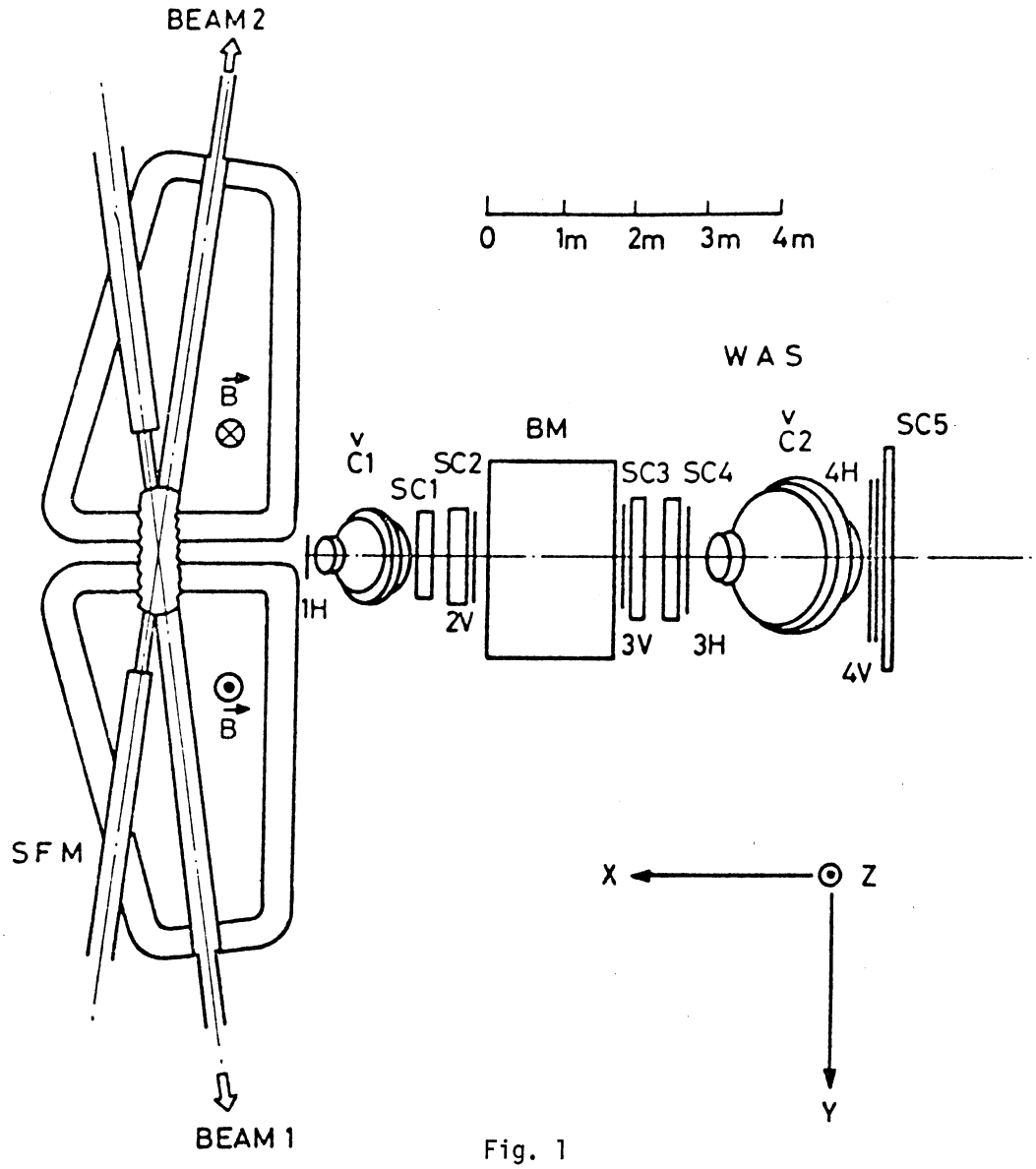
BEAM 2
0
1m
2m
3m
4m
W A S
B
V
C1
SC1
SC2
BM
SC3
SC4
V
C2
4H
SC5
1H
2V
3V
3H
4V
B
SFM
X
Z
Y
BEAM 1

Fig. 1

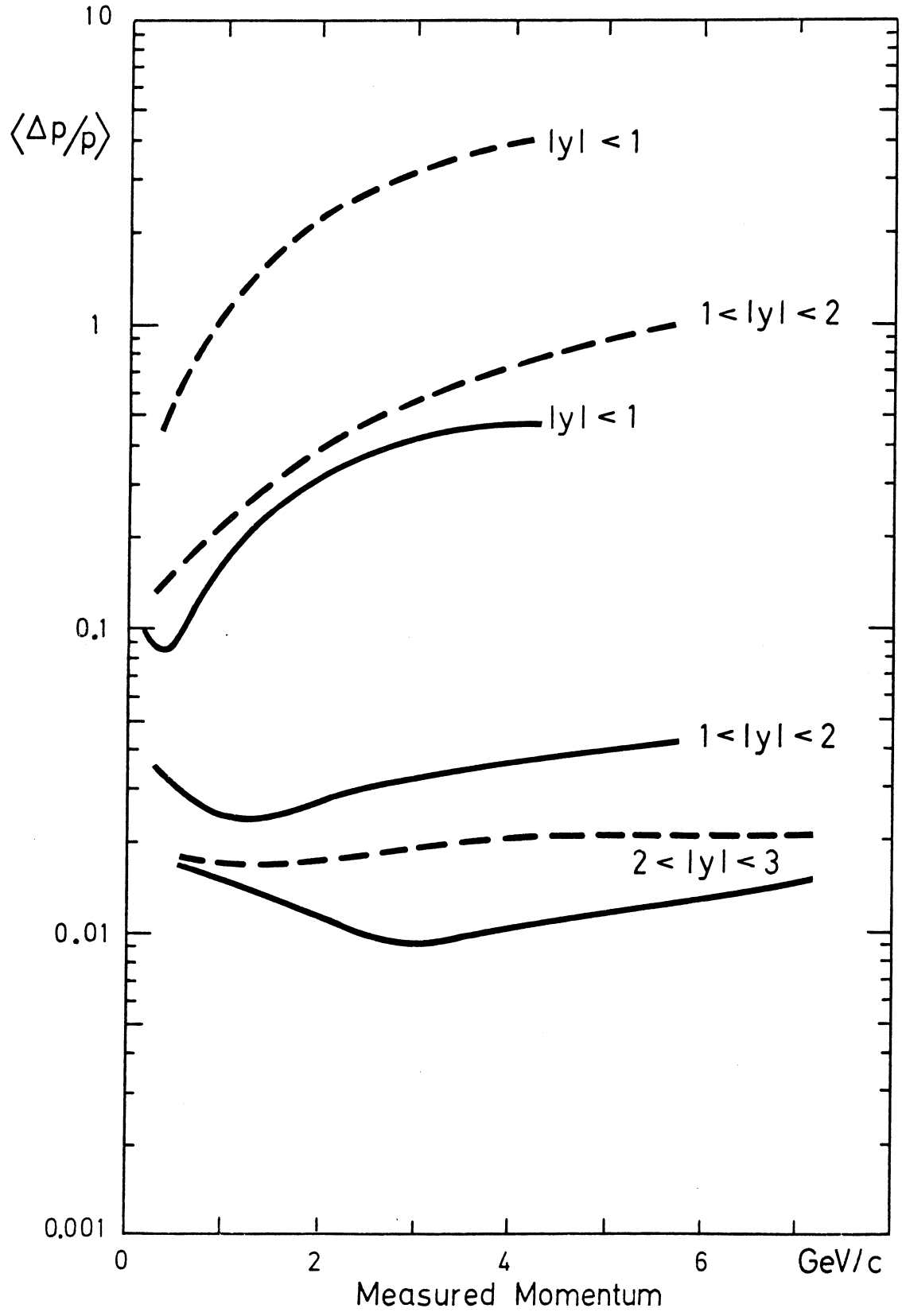
10
1
0.1
0.01
0.001
⟨Δp/p⟩
|y| < 1
1 < |y| < 2
|y| < 1
1 < |y| < 2
2 < |y| < 3
0
2
4
6
GeV/c
Measured Momentum

Fig. 2

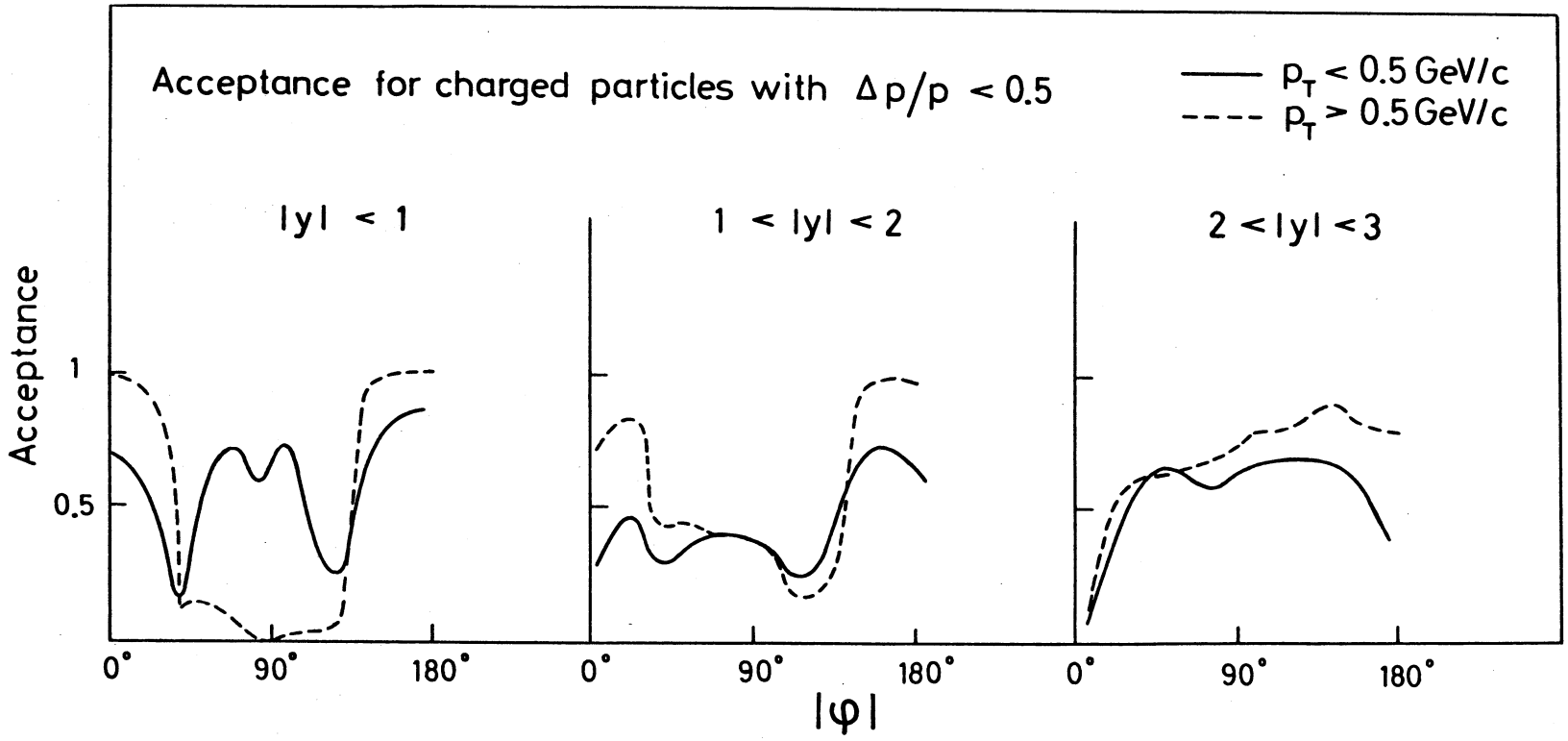
Acceptance for charged particles with Δp/p < 0.5
p_T < 0.5 GeV/c
p_T > 0.5 GeV/c
|y| < 1
1 < |y| < 2
2 < |y| < 3
Acceptance
1
0.5
0°
90°
180°
|φ|

Fig. 3

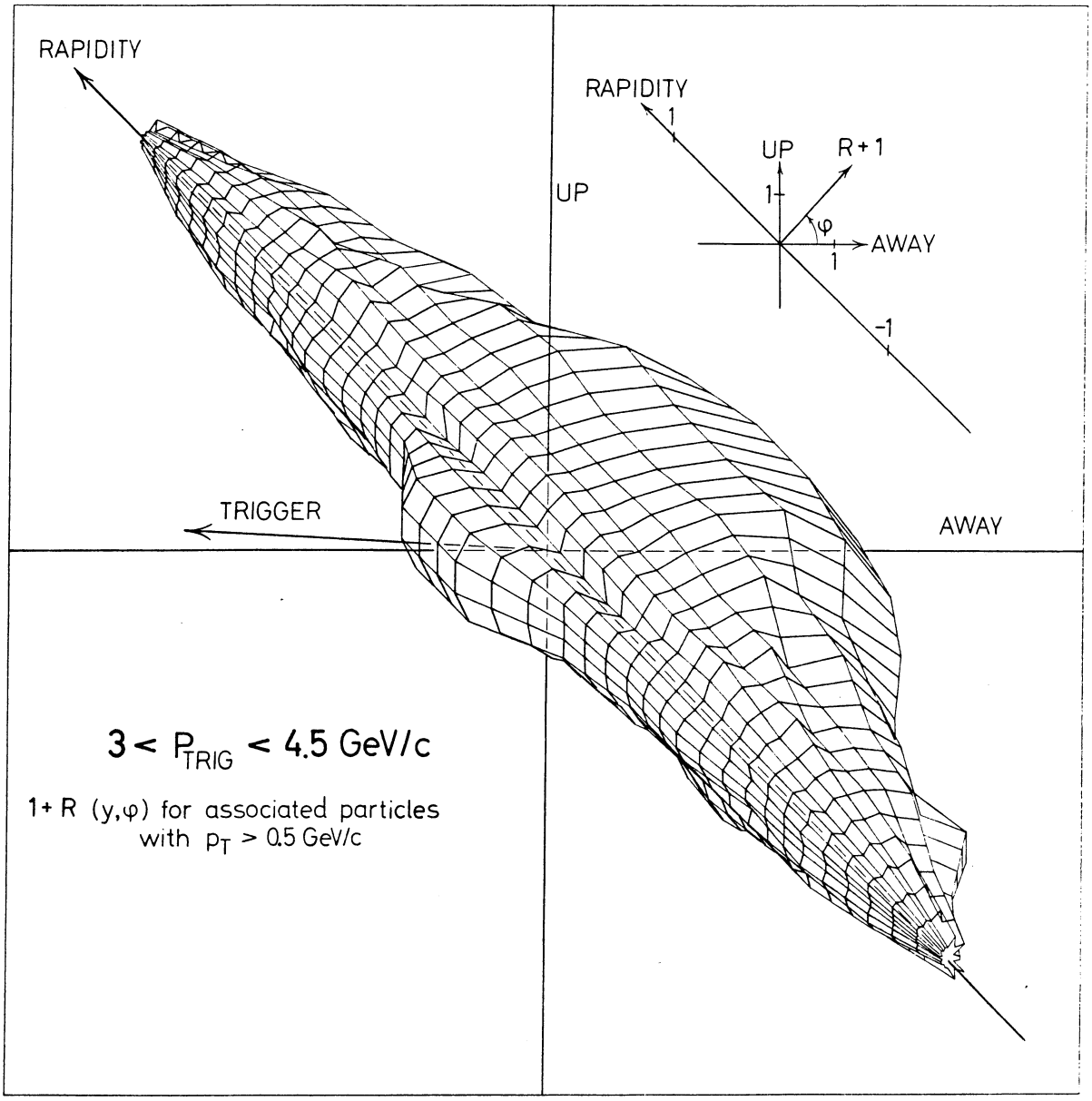
RAPIDITY
RAPIDITY
1
UP
R+1
UP
1
φ
AWAY
1
-1
TRIGGER
AWAY
3 < P_TRIG < 4.5 GeV/c
1+ R (y,φ) for associated particles
with p_T > 0.5 GeV/c

Fig. 4

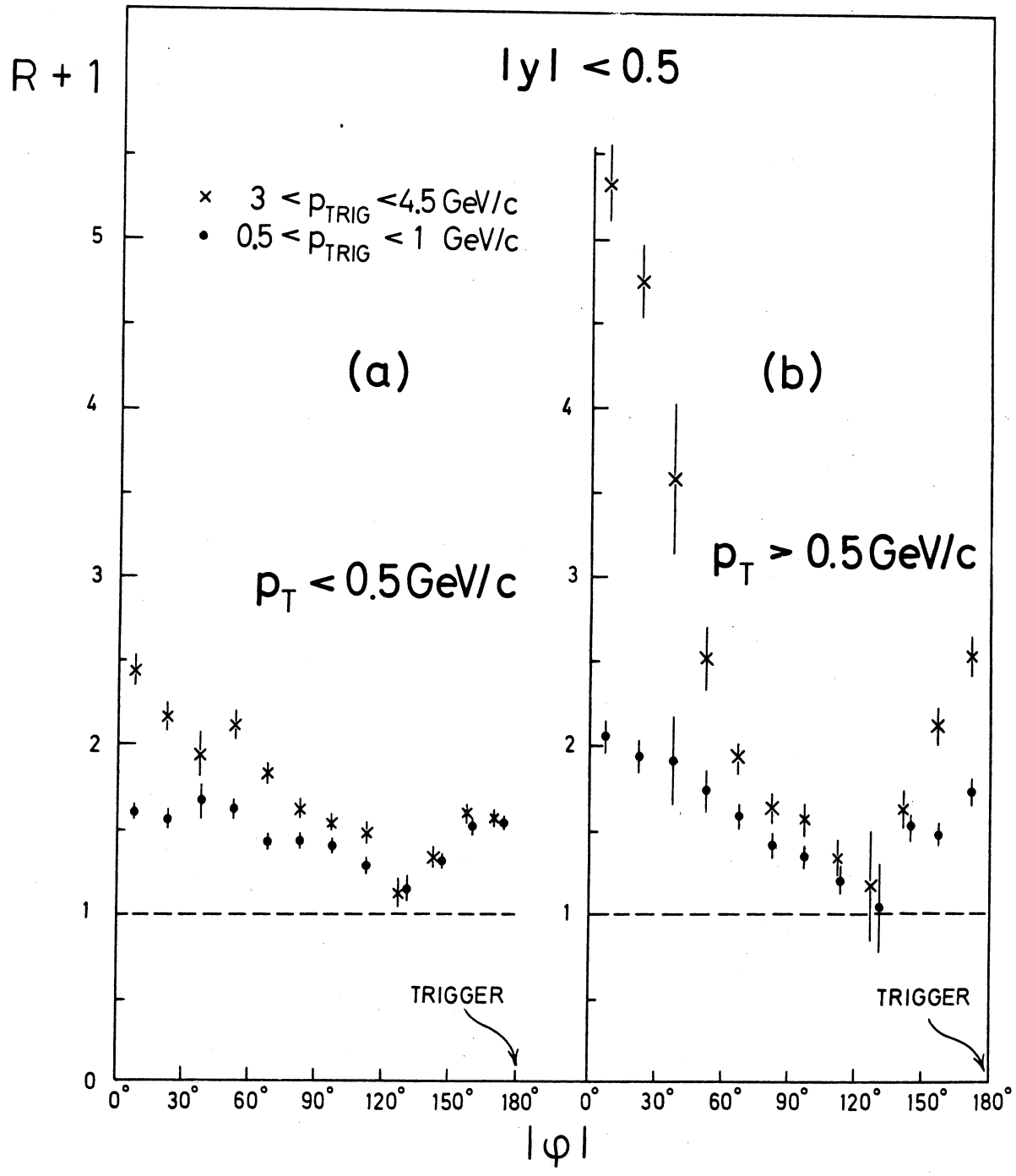
R + 1
|y| < 0.5
× 3 < p_TRIG < 4.5 GeV/c
• 0.5 < p_TRIG < 1 GeV/c
(a)
(b)
p_T < 0.5 GeV/c
p_T > 0.5 GeV/c
TRIGGER
TRIGGER
0
1
2
3
4
5
0° 30° 60° 90° 120° 150° 180°
|φ|

Fig. 5

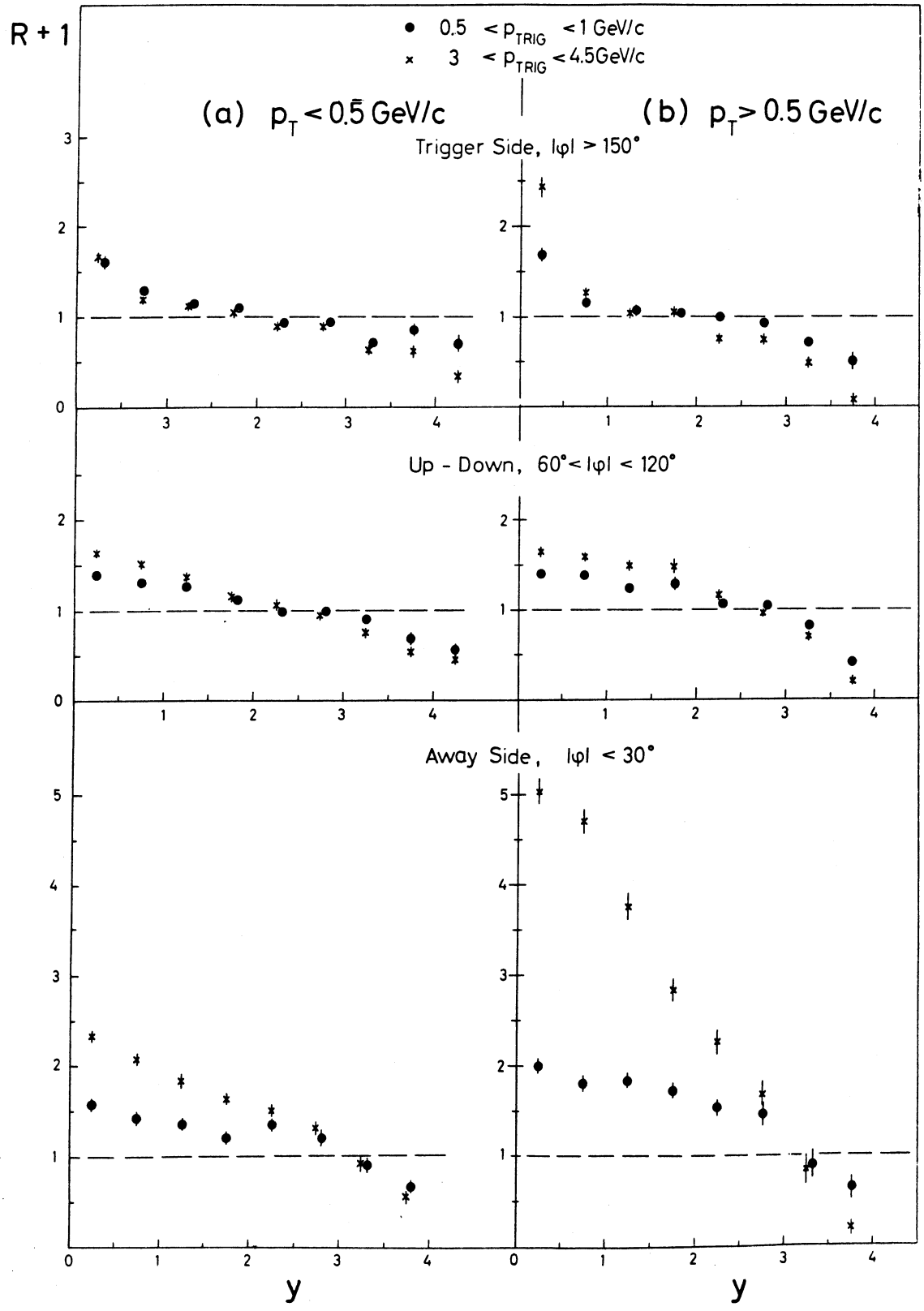
R + 1
● 0.5 < p_{TRIG} < 1 GeV/c
× 3 < p_{TRIG} < 4.5GeV/c
(a) p_T < 0.5 GeV/c
(b) p_T > 0.5 GeV/c
Trigger Side, |φ| > 150°
Up - Down, 60° < |φ| < 120°
Away Side, |φ| < 30°
y
y

Fig. 6

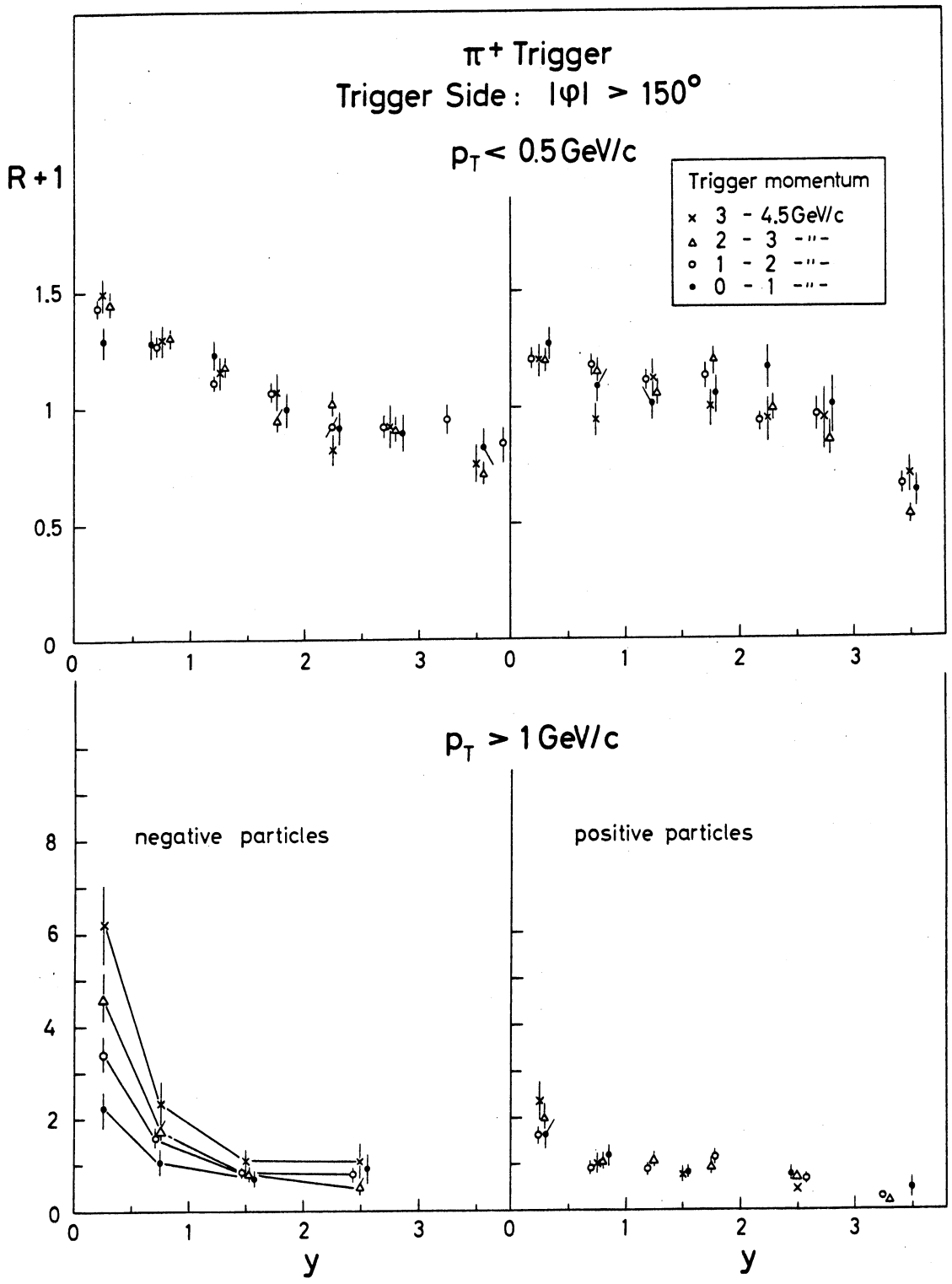
π+ Trigger
Trigger Side : |φ| > 150°
p_T < 0.5 GeV/c
R + 1
Trigger momentum
× 3 - 4.5 GeV/c
△ 2 - 3 -"-
○ 1 - 2 -"-
• 0 - 1 -"-
p_T > 1 GeV/c
negative particles
positive particles
y
y

Fig. 7a

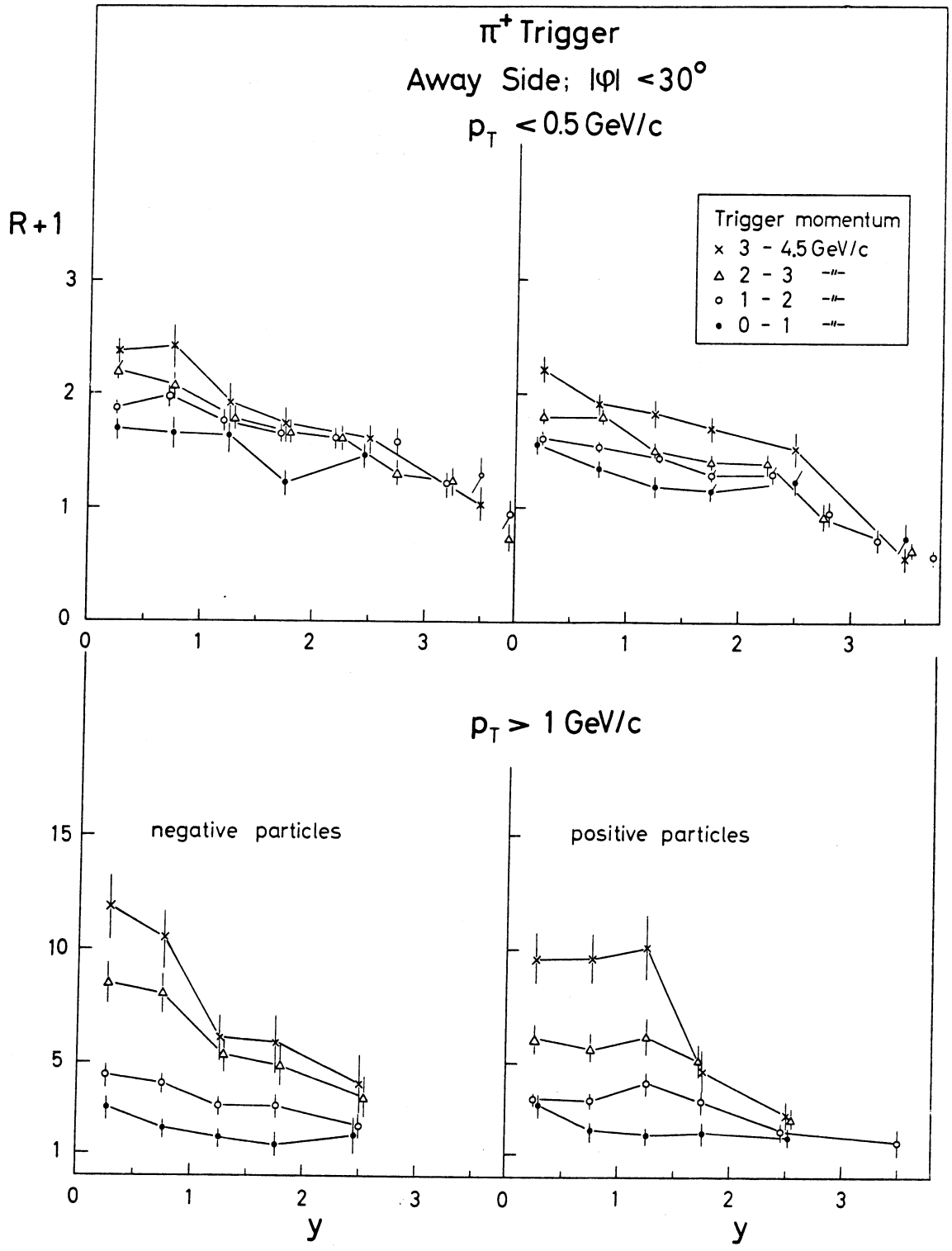
π+ Trigger
Away Side; |φ| <30°
pT <0.5 GeV/c
R+1
Trigger momentum
× 3 - 4.5 GeV/c
△ 2 - 3 -"-
○ 1 - 2 -"-
• 0 - 1 -"-
pT > 1 GeV/c
negative particles
positive particles
y
y

Fig. 7b

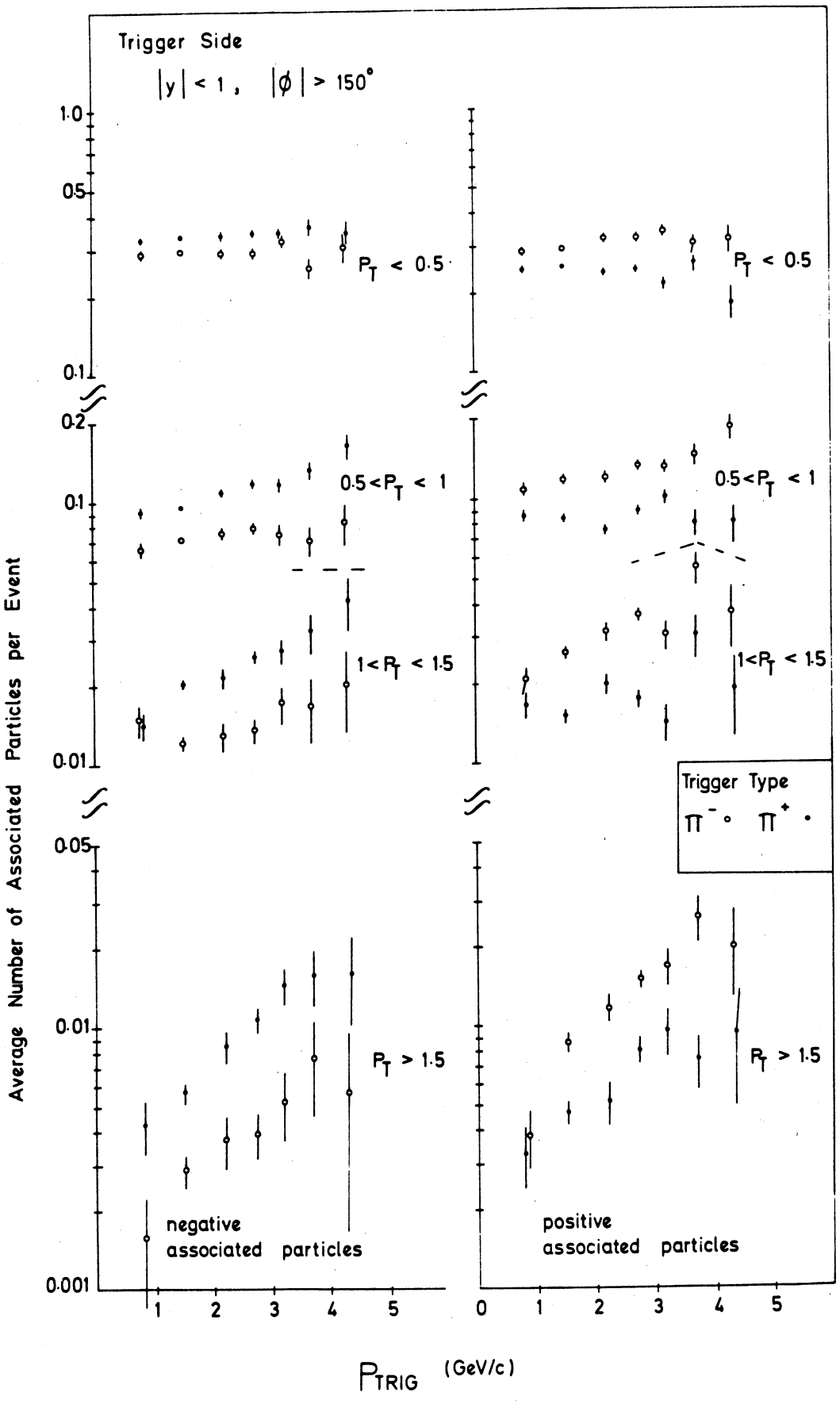
Trigger Side
|y| < 1 , |φ| > 150°
Average Number of Associated Particles per Event
P_T < 0.5
0.5<P_T < 1
1<P_T < 1.5
P_T > 1.5
Trigger Type
π⁻ ∘ π⁺ •
negative associated particles
positive associated particles
P_TRIG (GeV/c)

Fig. 8a

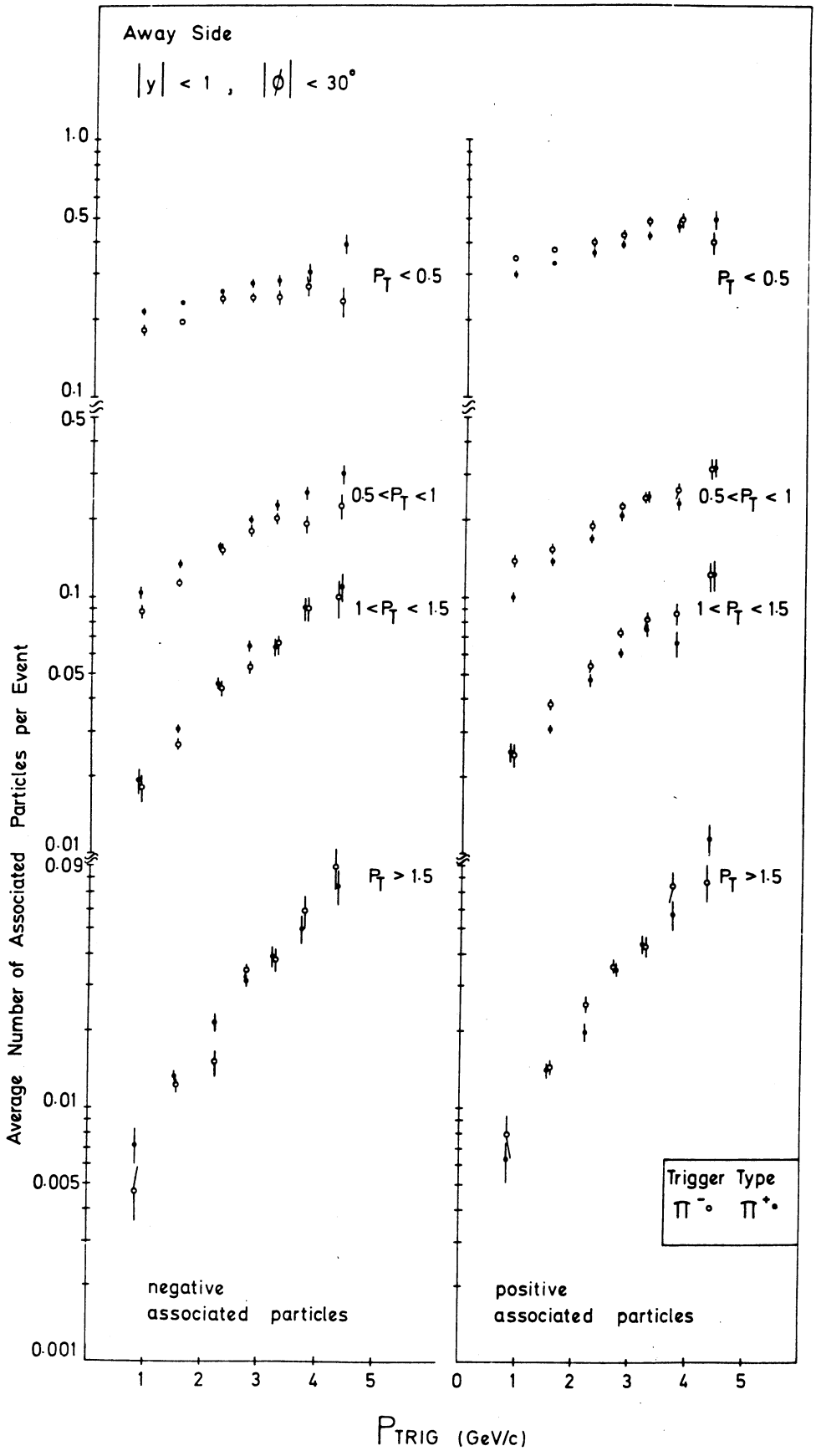
Away Side
|y| < 1 , |φ| < 30°
P_T < 0.5
0.5<P_T < 1
1 < P_T < 1.5
P_T > 1.5
Trigger Type
π⁻ π⁺
negative associated particles
positive associated particles
Average Number of Associated Particles per Event
P_TRIG (GeV/c)

Fig. 8b

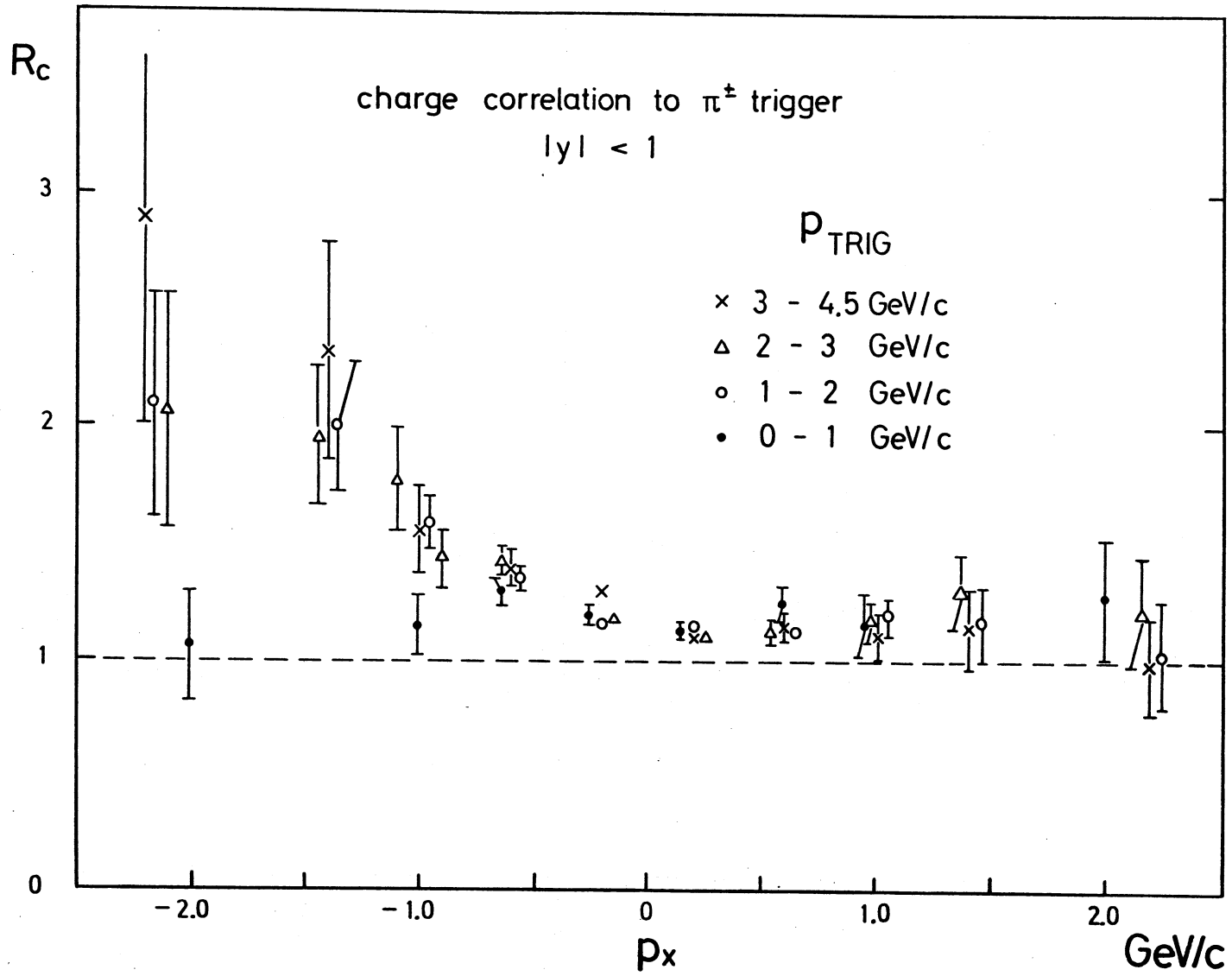
R_c
charge correlation to $\pi^{\pm}$ trigger
|y| < 1
p_{TRIG}
× 3 - 4.5 GeV/c
△ 2 - 3 GeV/c
○ 1 - 2 GeV/c
• 0 - 1 GeV/c
3
2
1
0
−2.0
−1.0
0
1.0
2.0
p_x
GeV/c

Fig. 9

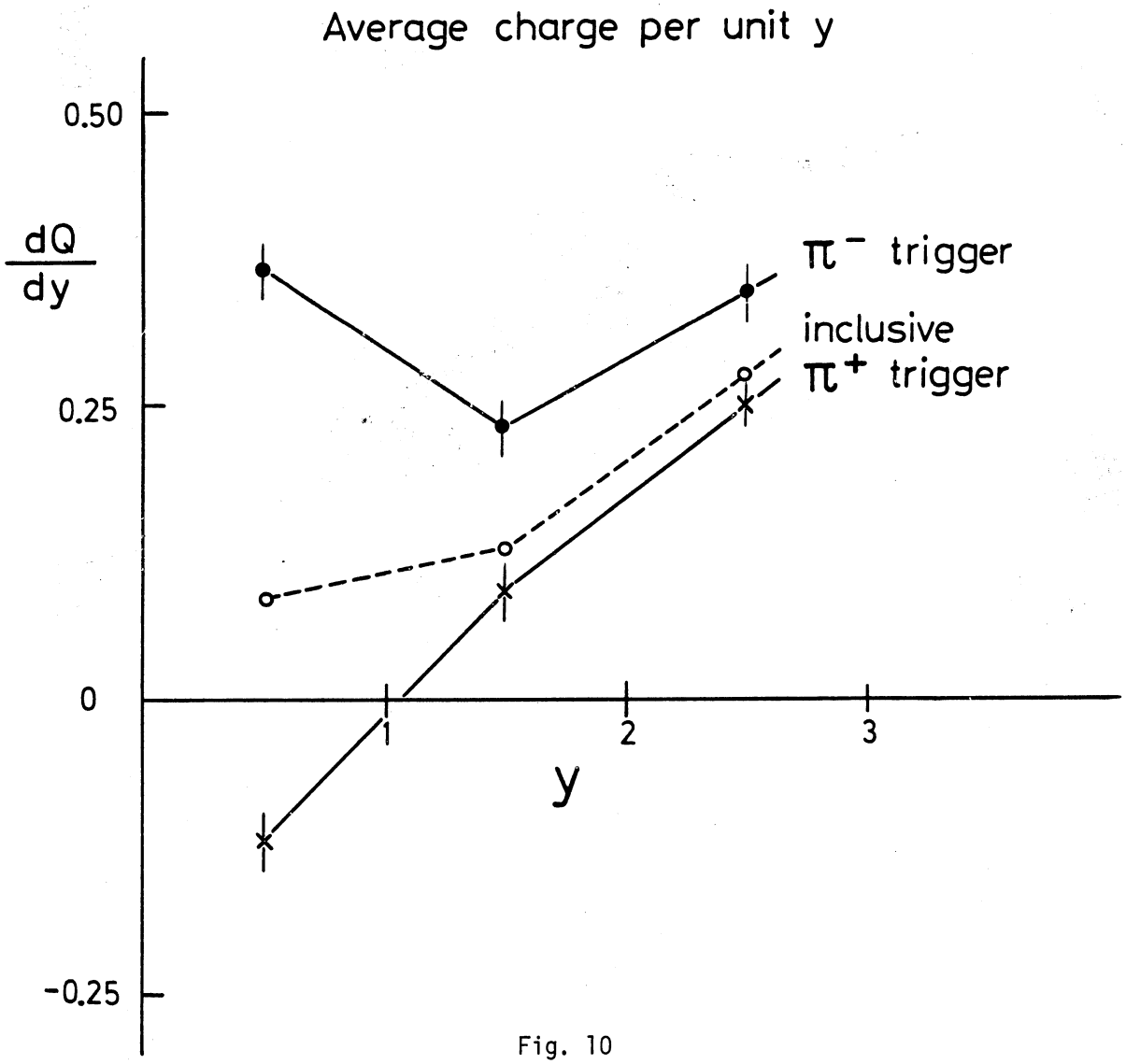
Average charge per unit y
0.50
dQ/dy
0.25
0
-0.25
1
2
3
y
π⁻ trigger
inclusive
π⁺ trigger

Fig. 10

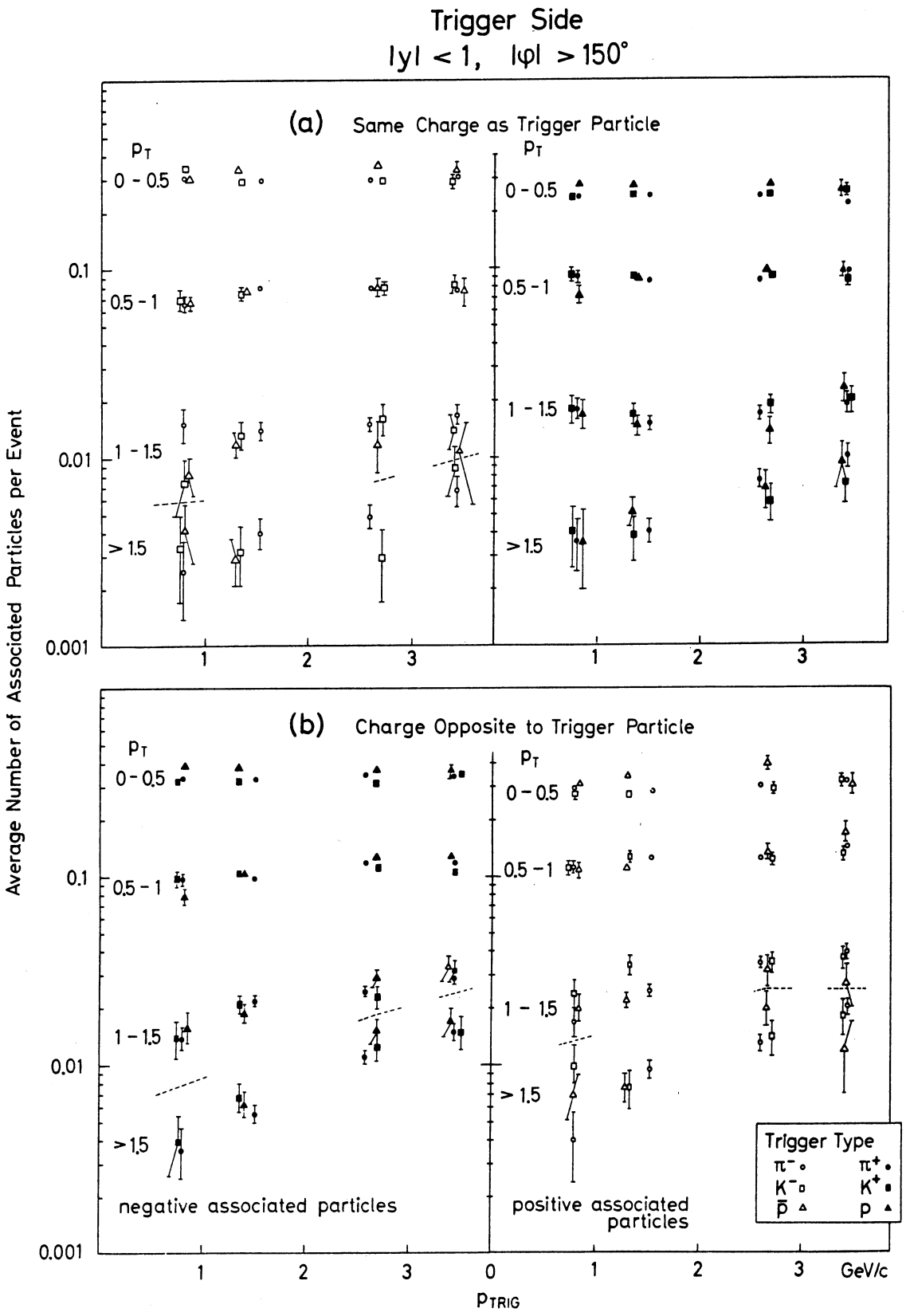
Trigger Side
|y| < 1, |φ| > 150°
(a) Same Charge as Trigger Particle
(b) Charge Opposite to Trigger Particle
p_T
0 - 0.5
0.5 - 1
1 - 1.5
> 1.5
Average Number of Associated Particles per Event
0.1
0.01
0.001
1
2
3
0
negative associated particles
positive associated particles
Trigger Type
π^- π^+
K^- K^+
$\bar{p}$ p
GeV/c
p_{TRIG}

Fig. 11a,b

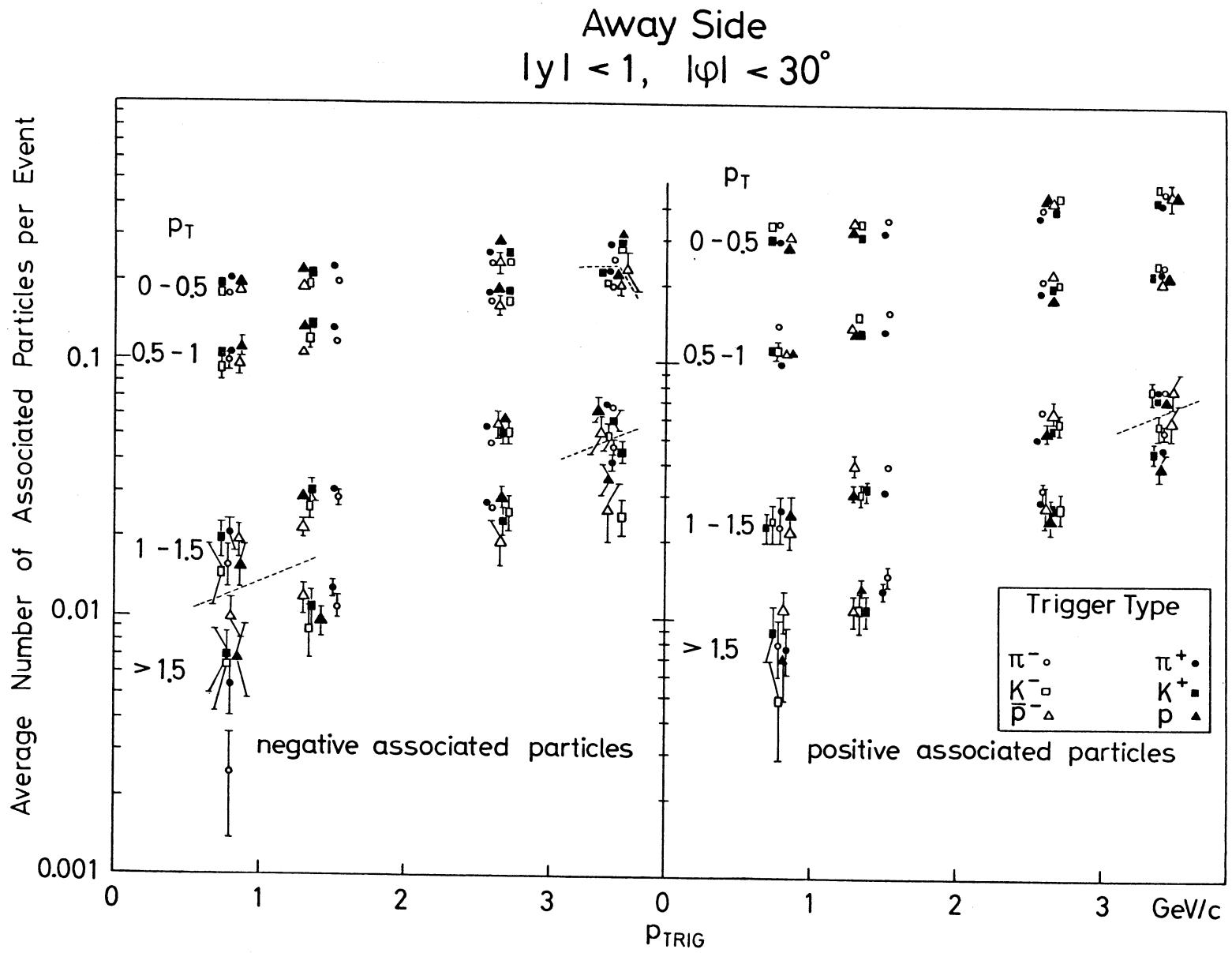
Away Side
|y| < 1, |φ| < 30°
Average Number of Associated Particles per Event
0.1
0.01
0.001
pT
0 - 0.5
0.5 - 1
1 - 1.5
> 1.5
negative associated particles
positive associated particles
Trigger Type
π⁻
K⁻
p̄⁻
π⁺
K⁺
p
0
1
2
3
GeV/c
pTRIG

Fig. 11c

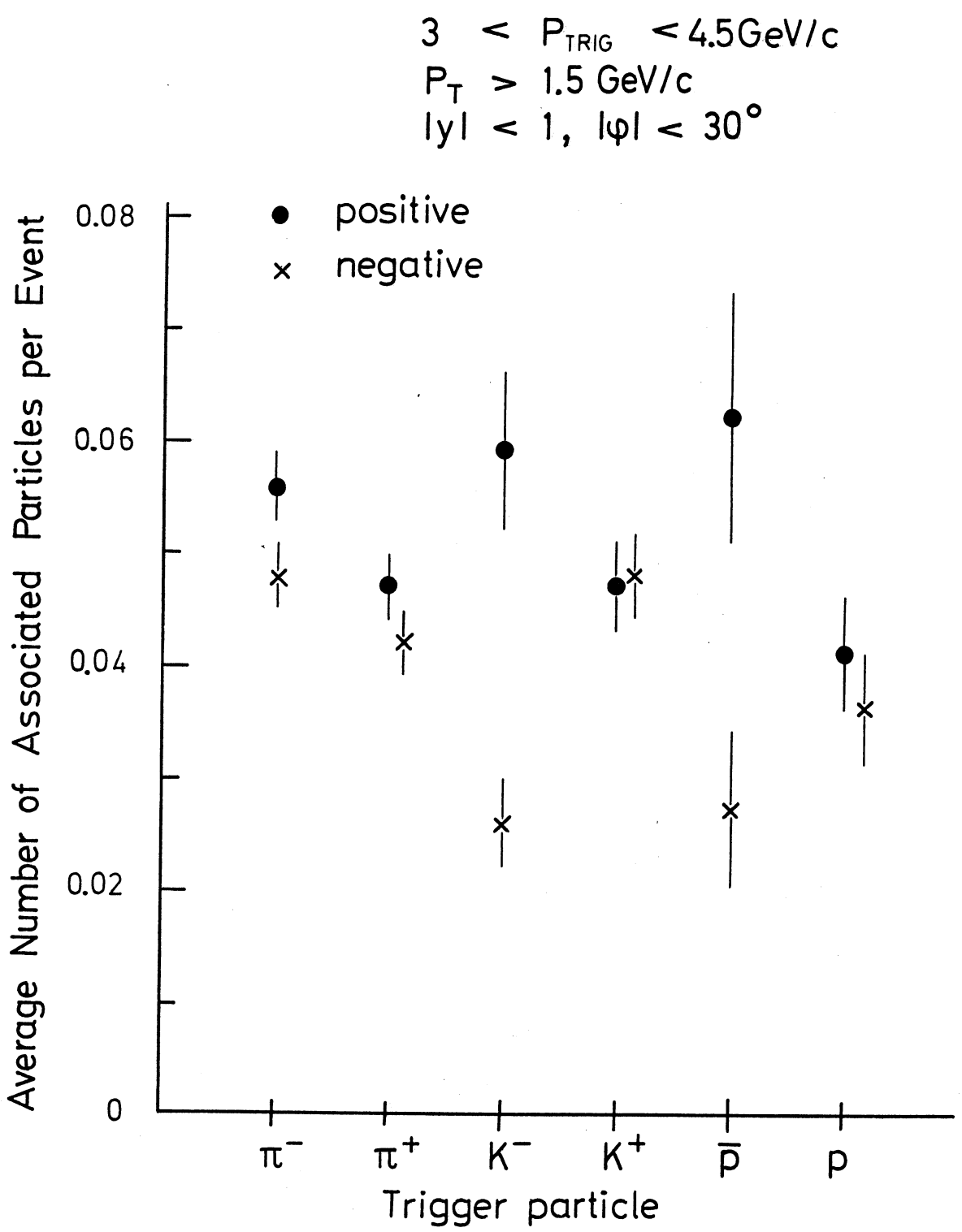
3 < P_{TRIG} < 4.5GeV/c
P_T > 1.5 GeV/c
|y| < 1, |φ| < 30°
positive
negative
Average Number of Associated Particles per Event
0.08
0.06
0.04
0.02
0
π^-
π^+
K^-
K^+
$\bar{p}$
p
Trigger particle

Fig. 12

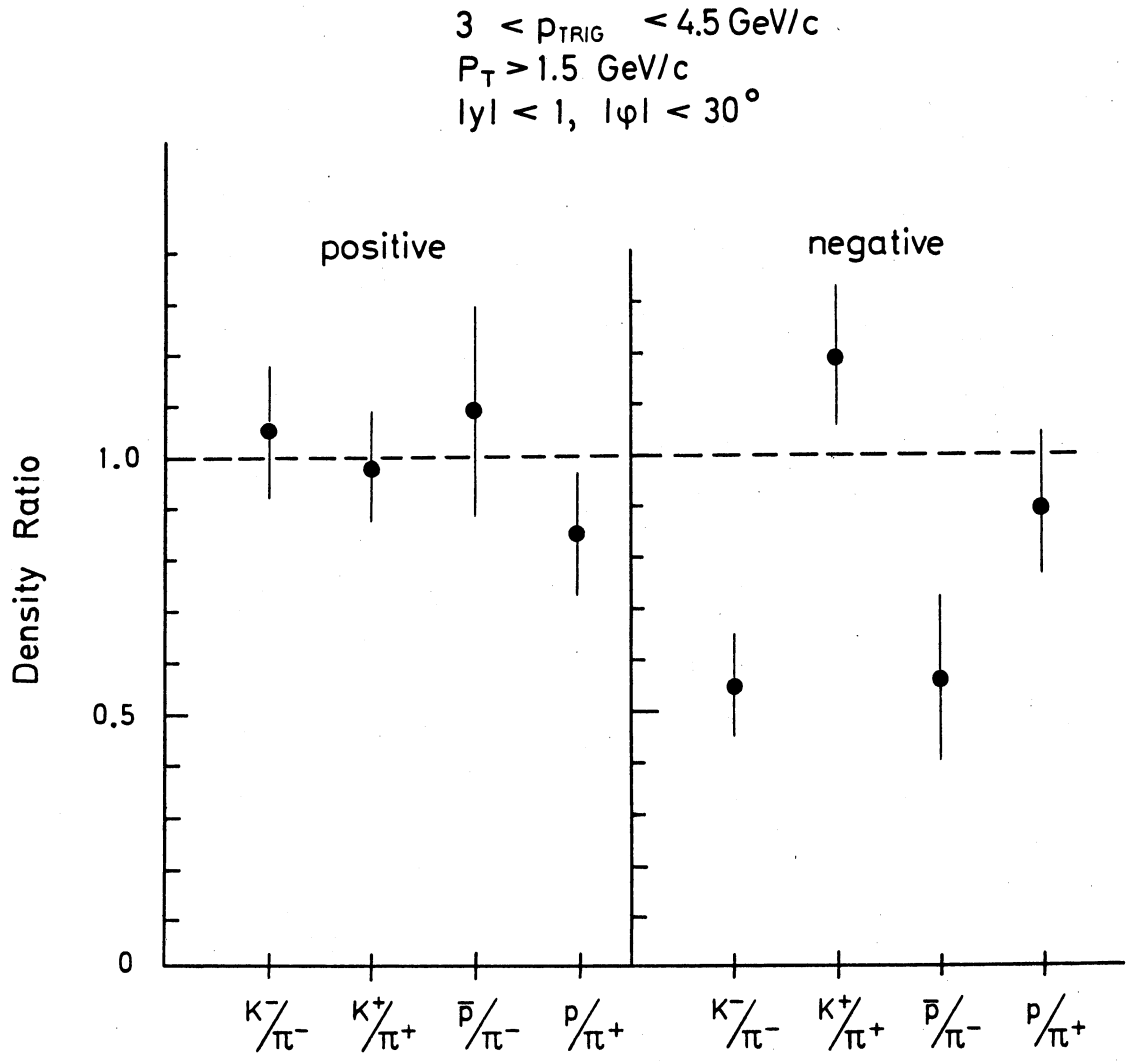
3 < p_{TRIG} < 4.5 GeV/c
P_T > 1.5 GeV/c
|y| < 1, |φ| < 30°
positive
negative
Density Ratio
1.0
0.5
0
K^-/π^-
K^+/π^+
$\bar{p}/\pi^-$
p/π^+
K^-/π^-
K^+/π^+
$\bar{p}/\pi^-$
p/π^+

Fig. 13

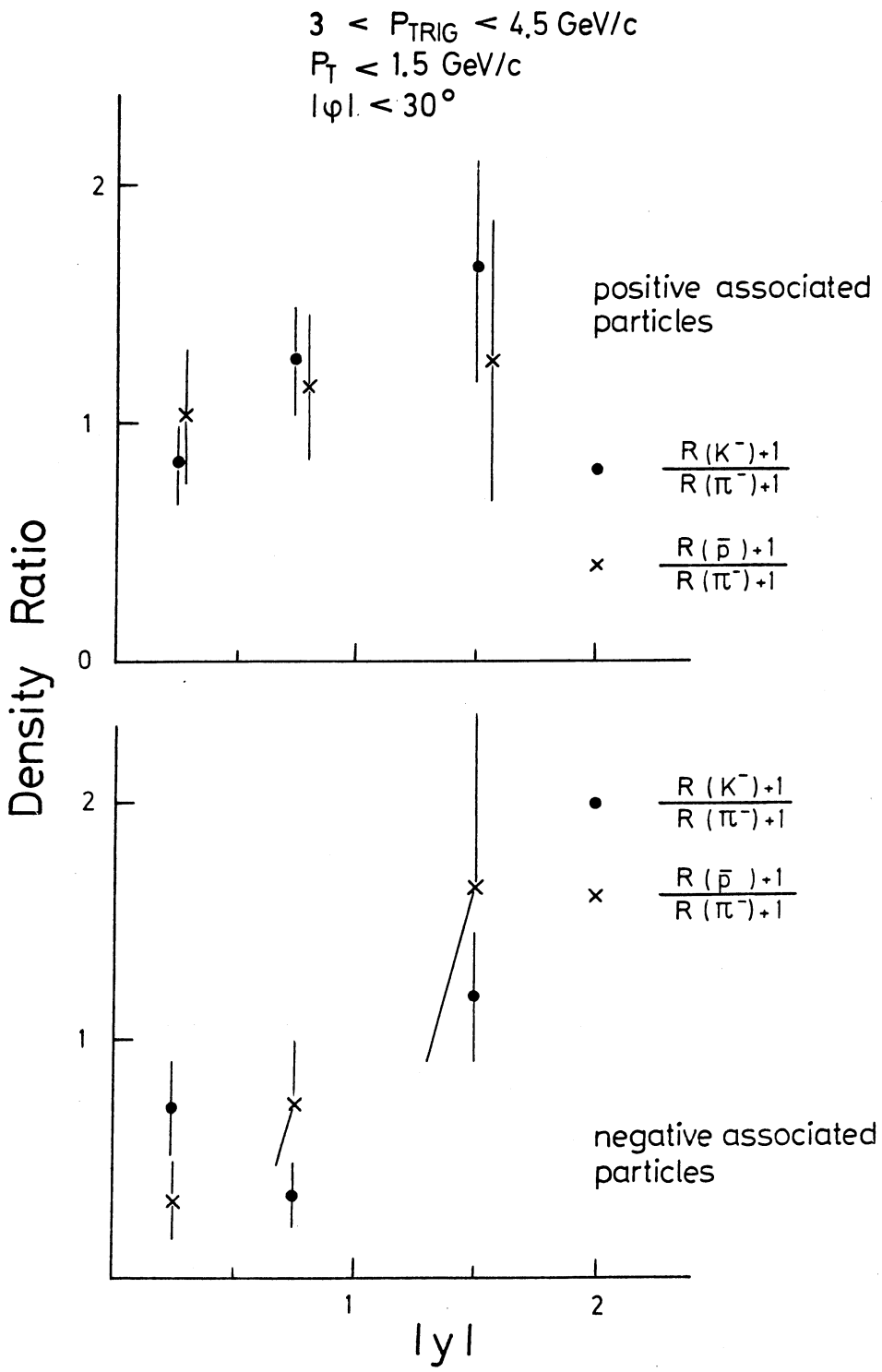
3 < P_TRIG < 4.5 GeV/c
P_T < 1.5 GeV/c
|φ| < 30°
Density Ratio
positive associated particles
R(K⁻)+1 / R(π⁻)+1
R(p̄)+1 / R(π⁻)+1
negative associated particles
R(K⁻)+1 / R(π⁻)+1
R(p̄)+1 / R(π⁻)+1
0
1
2
|y|

Fig. 14

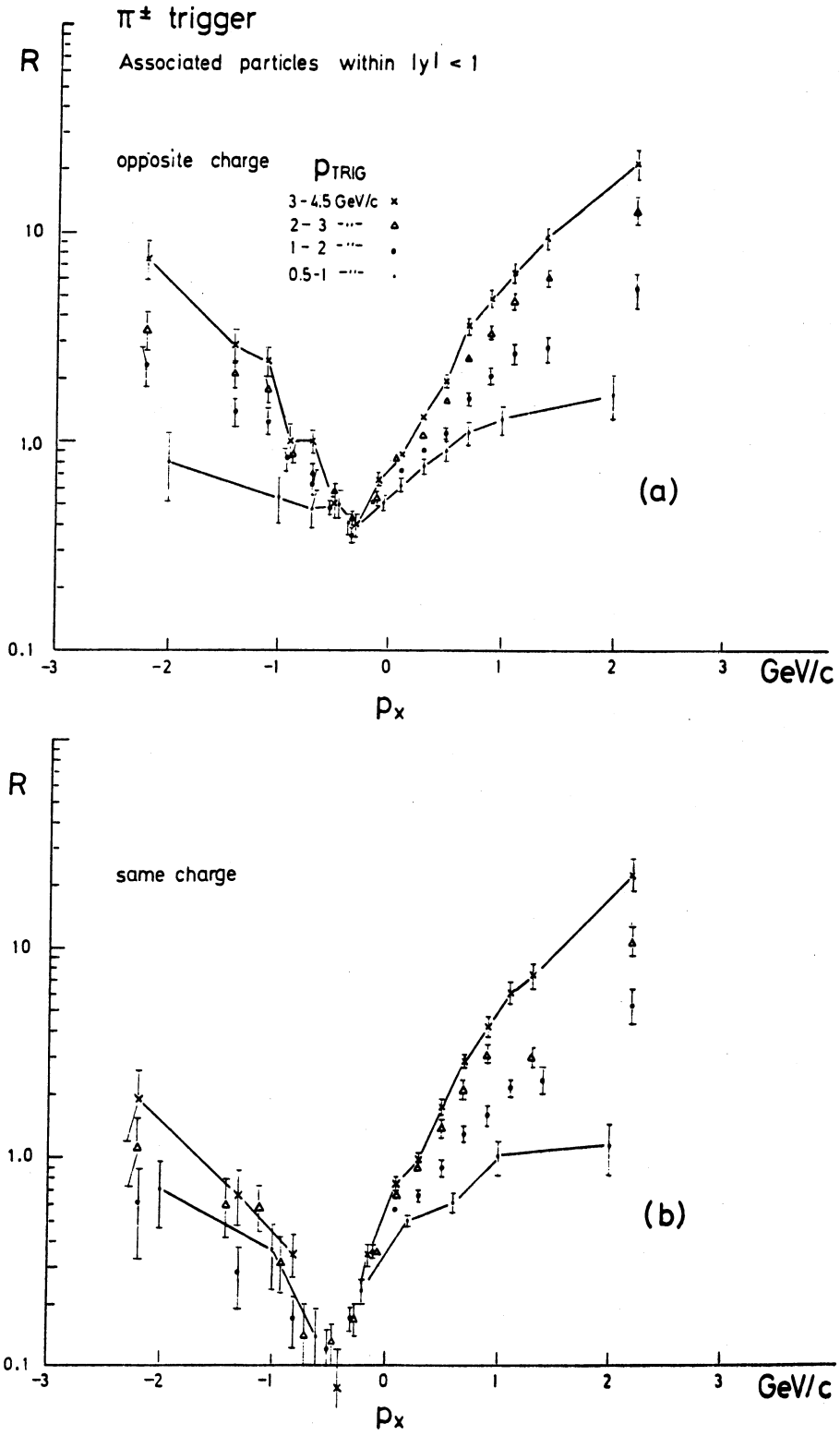
π± trigger
Associated particles within |y| < 1
opposite charge
p_{TRIG}
3 - 4.5 GeV/c
2 - 3
1 - 2
0.5 - 1
R
10
1.0
0.1
-3
-2
-1
0
1
2
3
GeV/c
p_x
(a)
same charge
(b)

Fig. 15

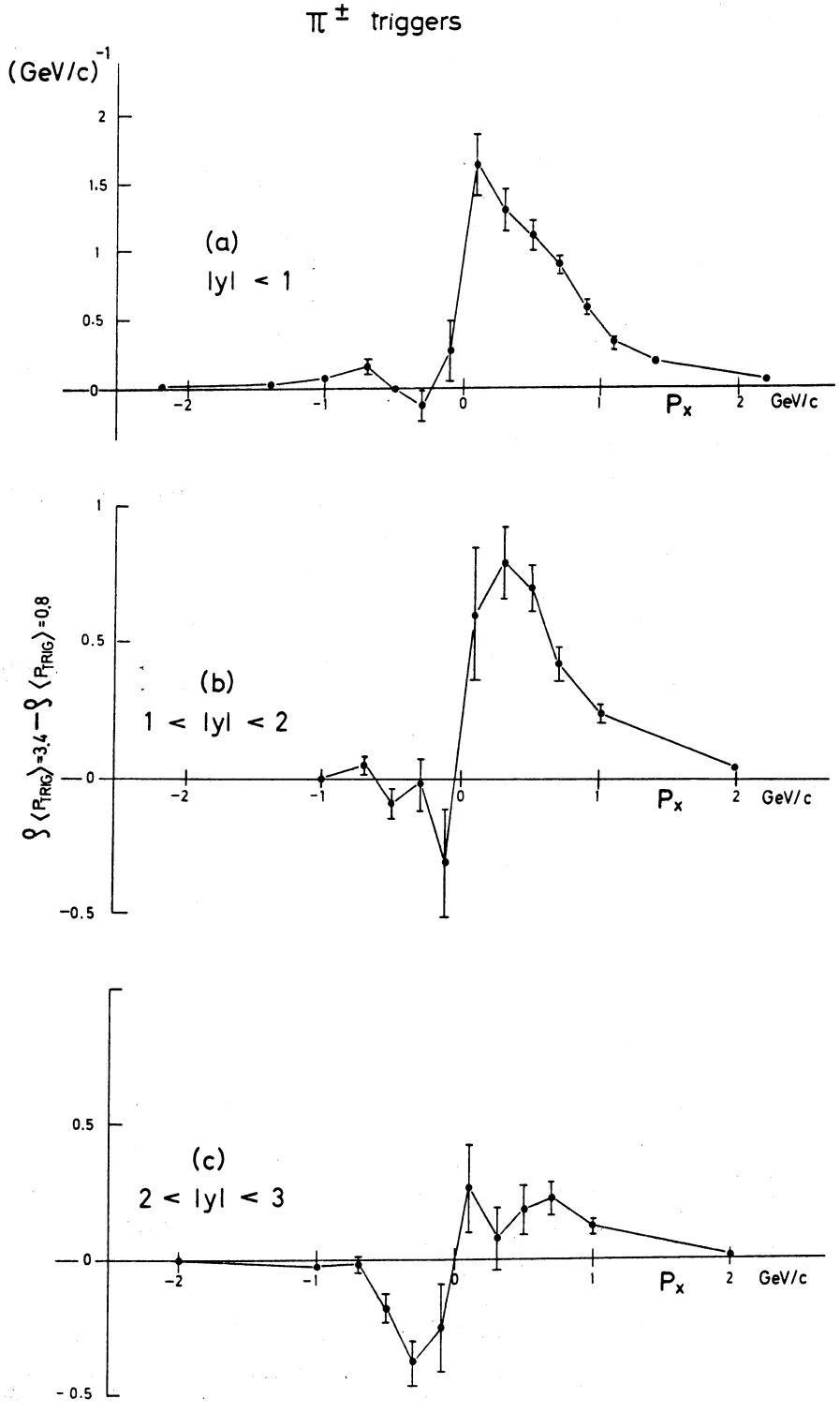

Fig. 16

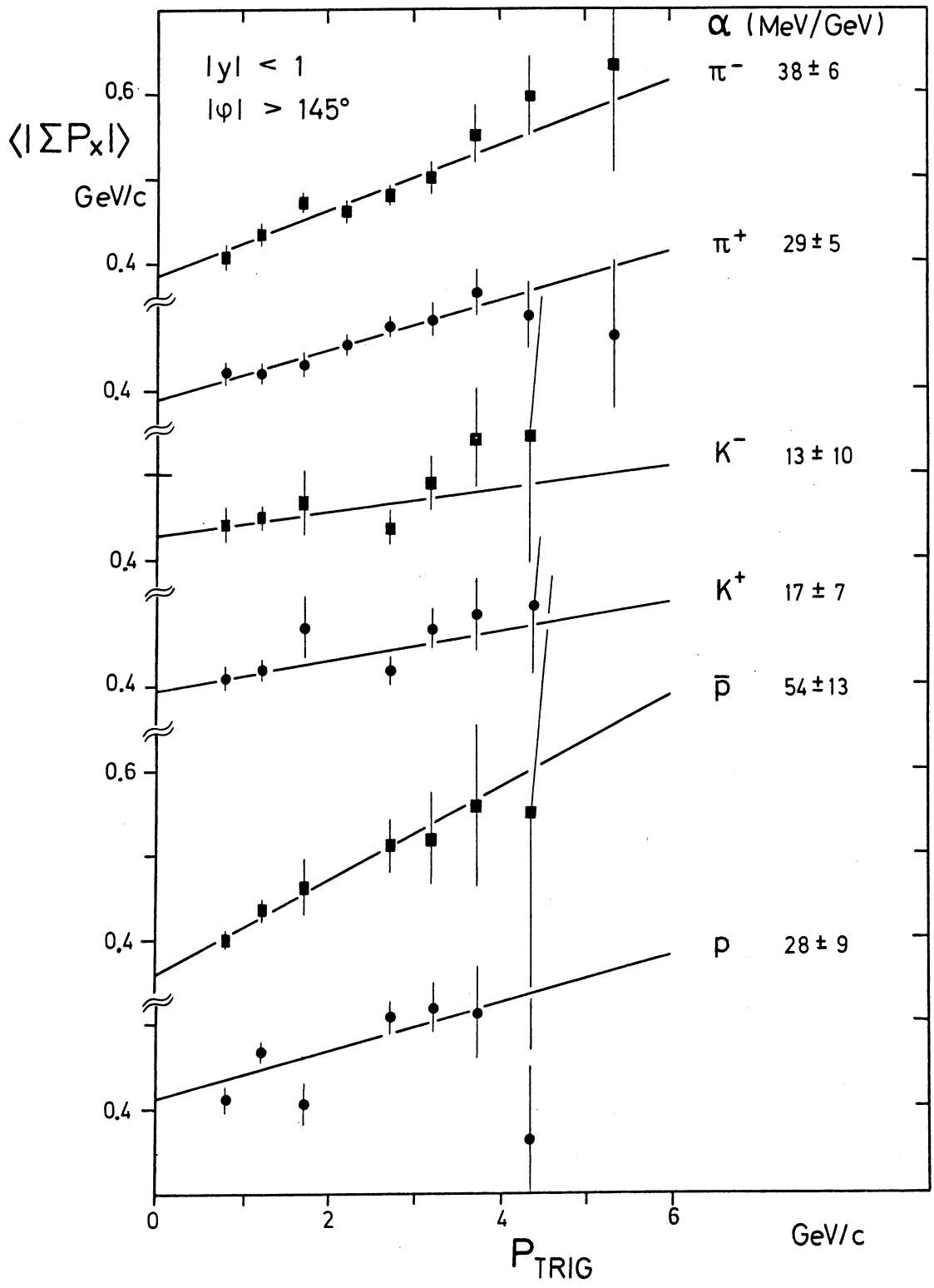
α (MeV/GeV)
|y| < 1
|φ| > 145°
⟨|ΣPx|⟩
GeV/c
π⁻ 38 ± 6
π⁺ 29 ± 5
K⁻ 13 ± 10
K⁺ 17 ± 7
p̄ 54 ± 13
p 28 ± 9
0.6
0.4
0.4
0.4
0.6
0.4
0.4
0
2
4
6
PTRIG
GeV/c

Fig. 17

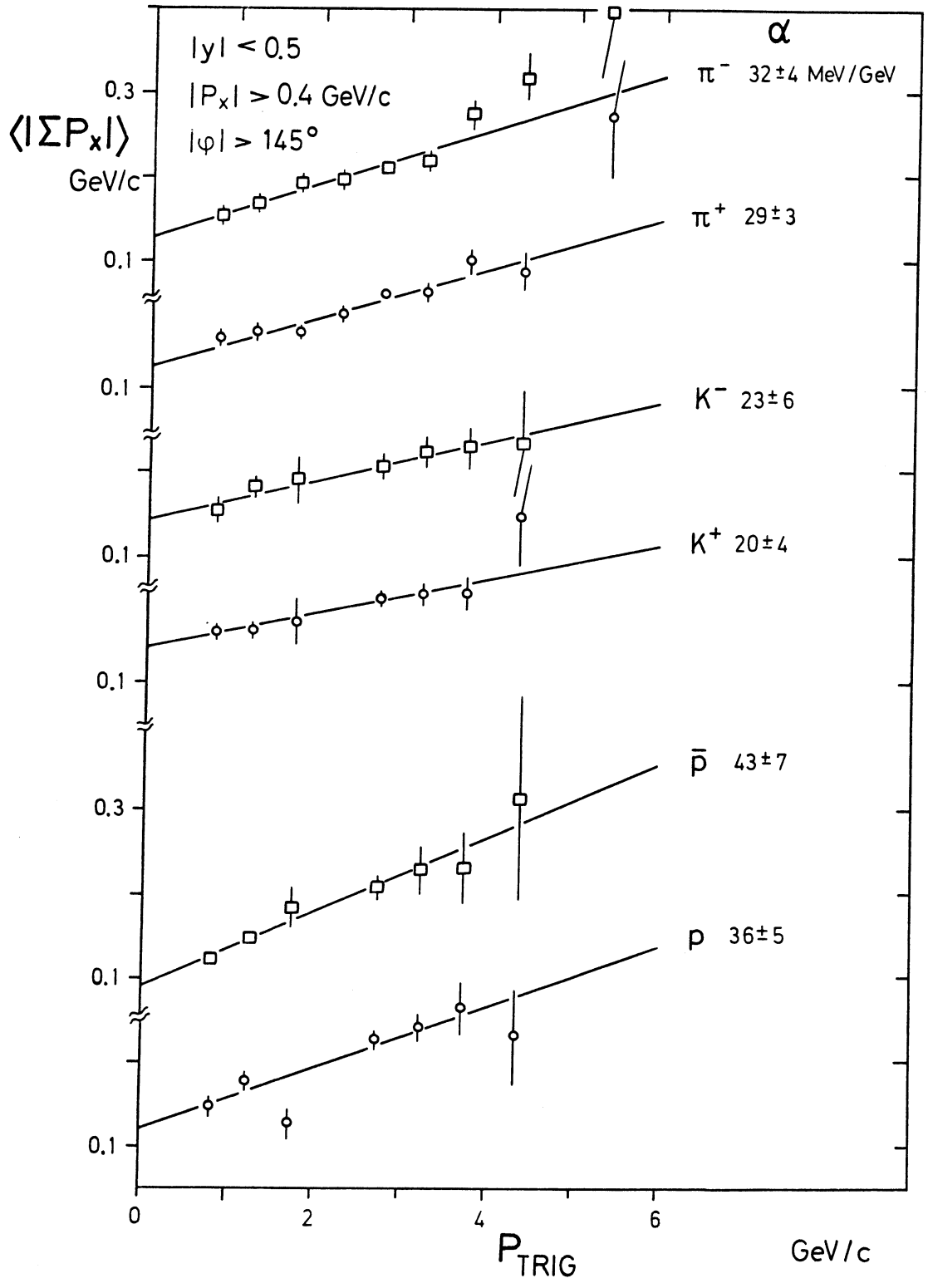
α
|y| < 0.5
|Px| > 0.4 GeV/c
|φ| > 145°
⟨|ΣPx|⟩
GeV/c
π⁻ 32±4 MeV/GeV
π⁺ 29±3
K⁻ 23±6
K⁺ 20±4
p̄ 43±7
p 36±5
0.3
0.1
0.1
0.1
0.1
0.3
0.1
0.1
0
2
4
6
PTRIG
GeV/c

Fig. 18

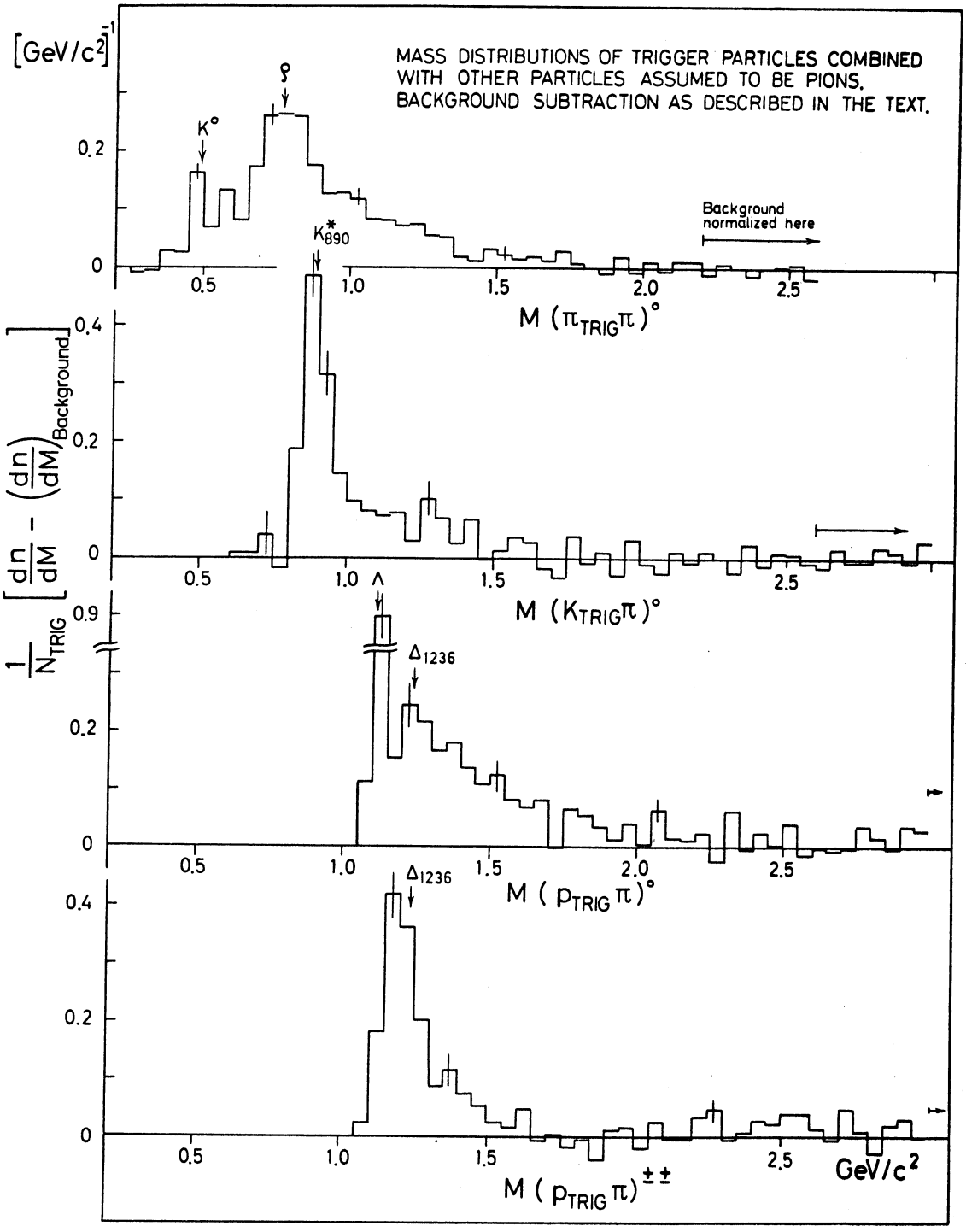
MASS DISTRIBUTIONS OF TRIGGER PARTICLES COMBINED WITH OTHER PARTICLES ASSUMED TO BE PIONS. BACKGROUND SUBTRACTION AS DESCRIBED IN THE TEXT.
[GeV/c²]⁻¹
K°
ρ
K*890
Background normalized here
M (πTRIGπ)°
[dn/dM − (dn/dM)Background]
M (KTRIGπ)°
1/NTRIG
Λ
Δ1236
M (pTRIGπ)°
M (pTRIGπ)±±
GeV/c²

Fig. 19

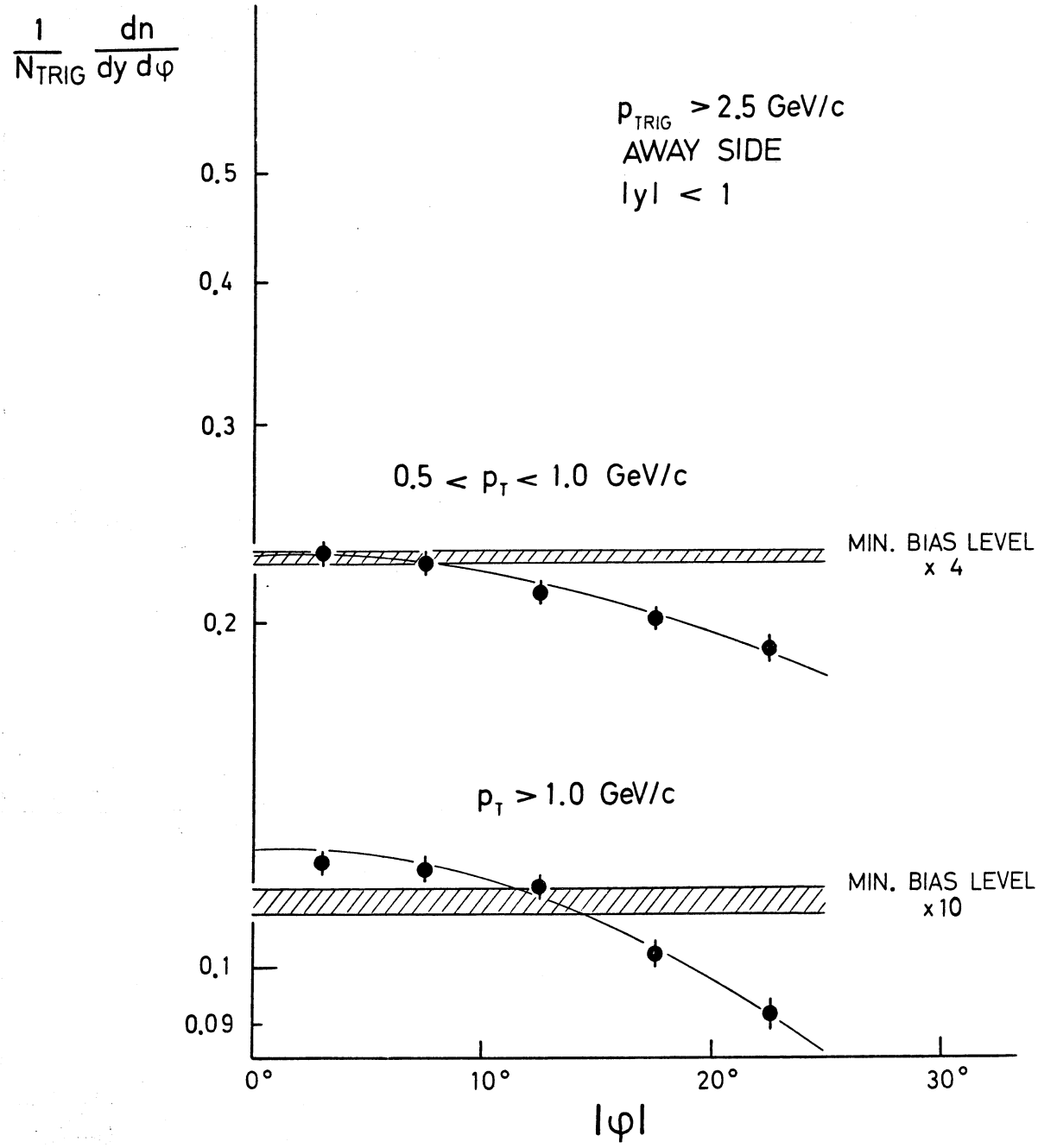
1/N_TRIG dn/dy dφ
p_TRIG > 2.5 GeV/c
AWAY SIDE
|y| < 1
0.5
0.4
0.3
0.5 < p_T < 1.0 GeV/c
MIN. BIAS LEVEL
x 4
0.2
p_T > 1.0 GeV/c
MIN. BIAS LEVEL
x 10
0.1
0.09
0°
10°
20°
30°
|φ|

Fig. 20

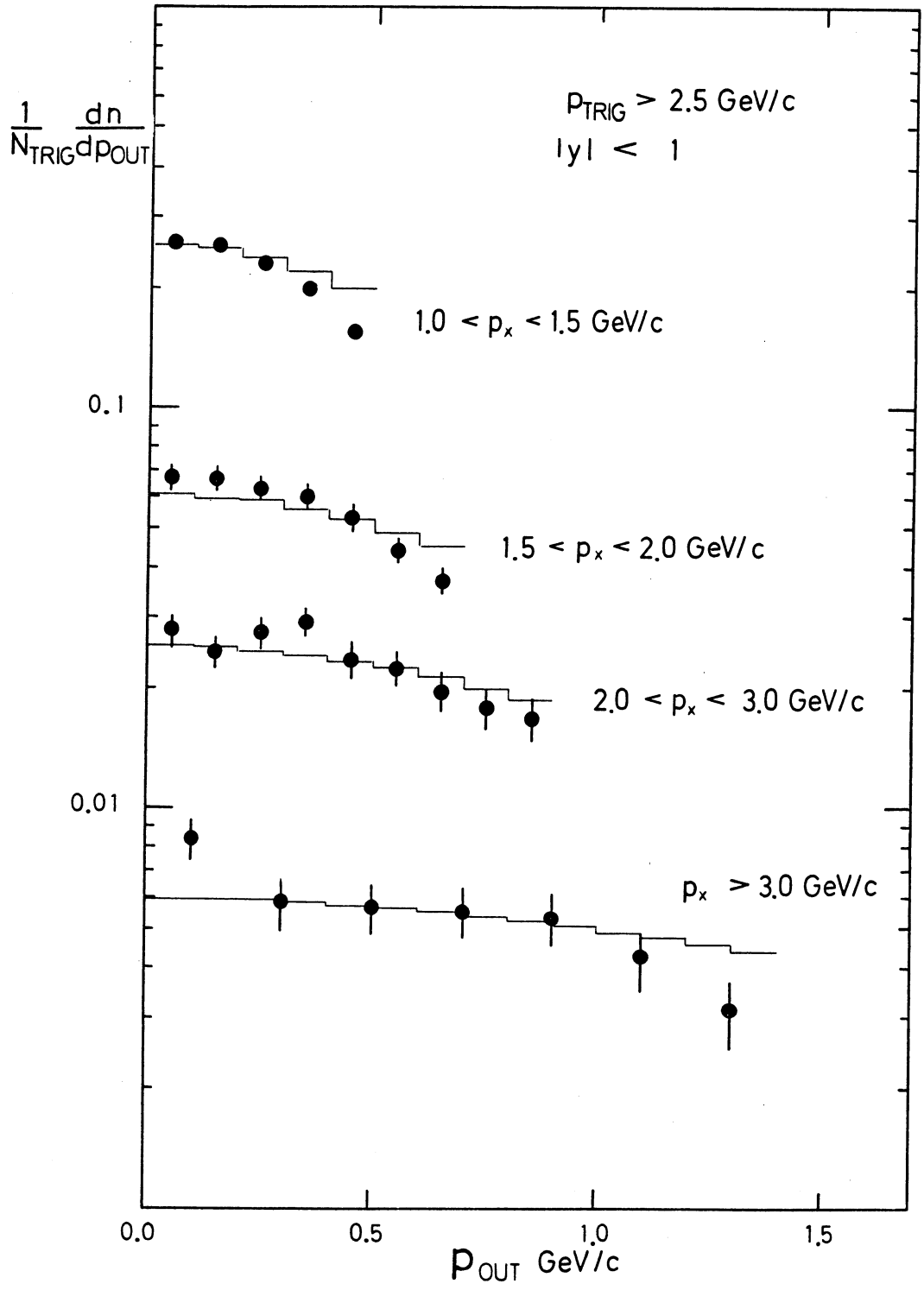
$\frac{1}{N_{TRIG}}\frac{dn}{dp_{OUT}}$
$p_{TRIG} > 2.5$ GeV/c
$|y| < 1$
$1.0 < p_x < 1.5$ GeV/c
$1.5 < p_x < 2.0$ GeV/c
$2.0 < p_x < 3.0$ GeV/c
$p_x > 3.0$ GeV/c
0.1
0.01
0.0
0.5
1.0
1.5
p_{OUT} GeV/c

Fig. 21

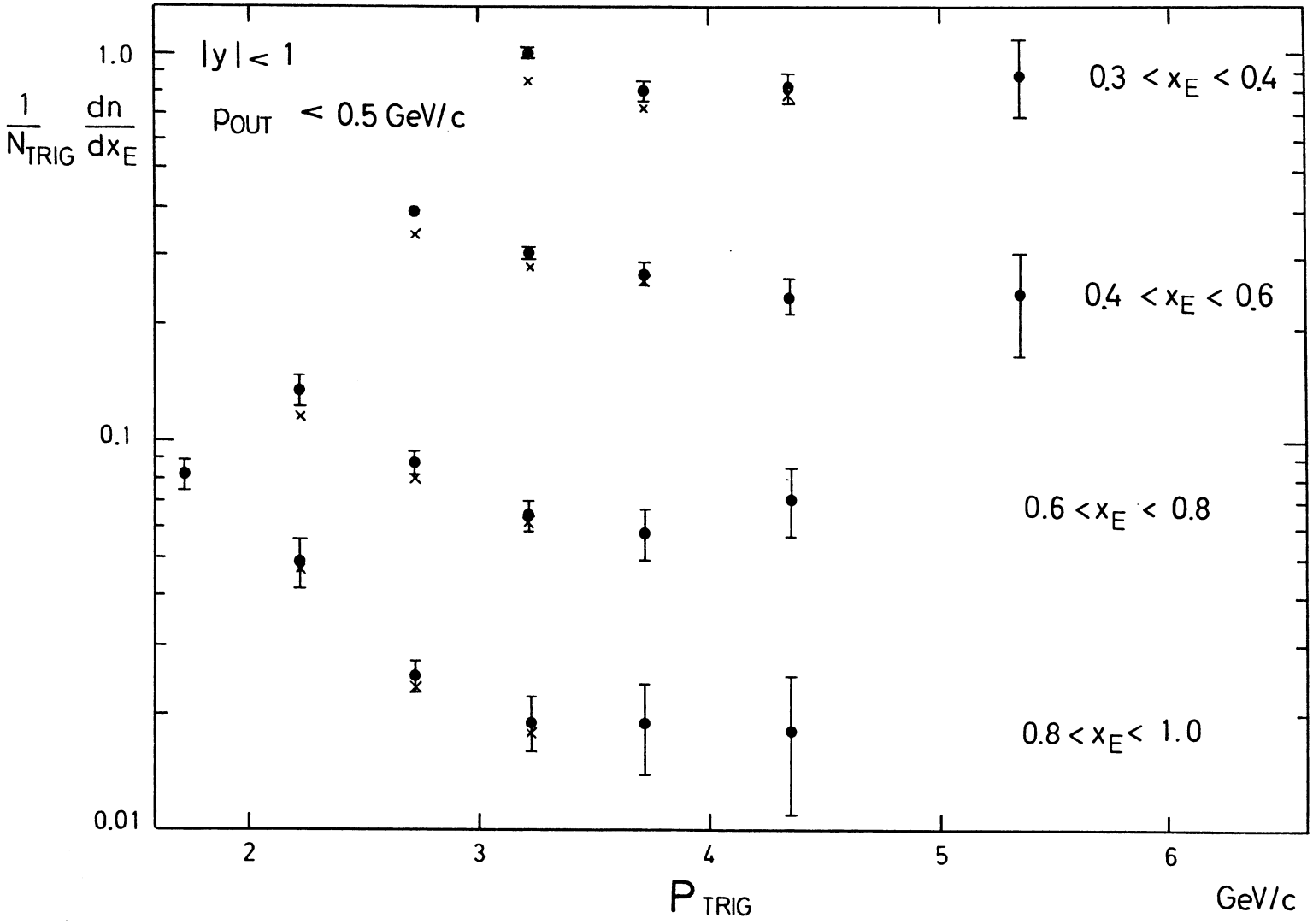
|y| < 1
P_{OUT} < 0.5 GeV/c
$\frac{1}{N_{TRIG}} \frac{dn}{dx_E}$
1.0
0.1
0.01
0.3 < x_E < 0.4
0.4 < x_E < 0.6
0.6 < x_E < 0.8
0.8 < x_E < 1.0
2
3
4
5
6
P_{TRIG}
GeV/c

Fig. 22

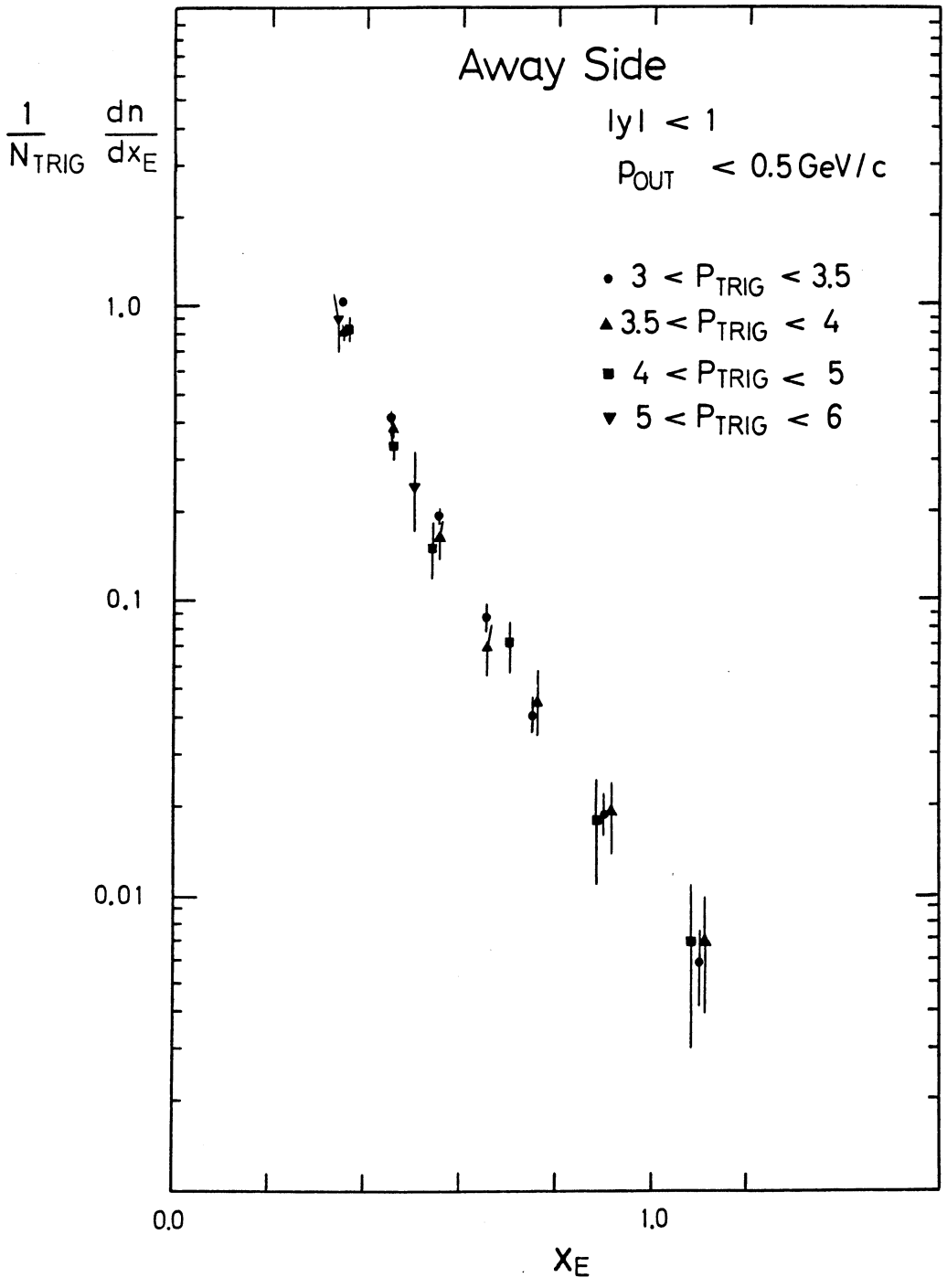
Away Side
|y| < 1
P_{OUT} < 0.5 GeV/c
• 3 < P_{TRIG} < 3.5
▲ 3.5 < P_{TRIG} < 4
■ 4 < P_{TRIG} < 5
▼ 5 < P_{TRIG} < 6
$\frac{1}{N_{TRIG}} \frac{dn}{dx_E}$
1.0
0.1
0.01
0.0
1.0
x_E

Fig. 23a

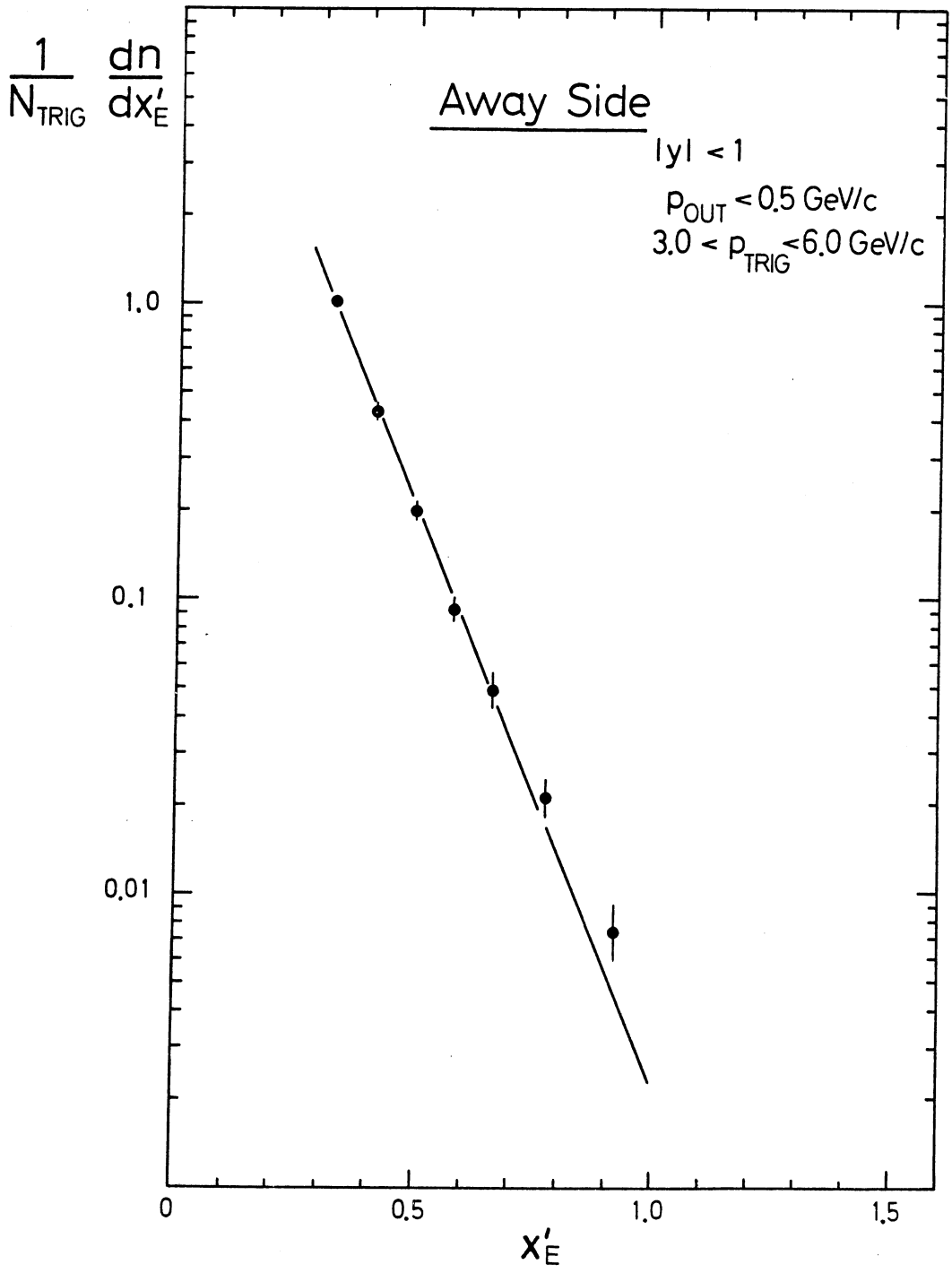
1/N_TRIG dn/dx'_E
Away Side
|y| < 1
p_OUT < 0.5 GeV/c
3.0 < p_TRIG < 6.0 GeV/c
1.0
0.1
0.01
0
0.5
1.0
1.5
x'_E

Fig. 23b

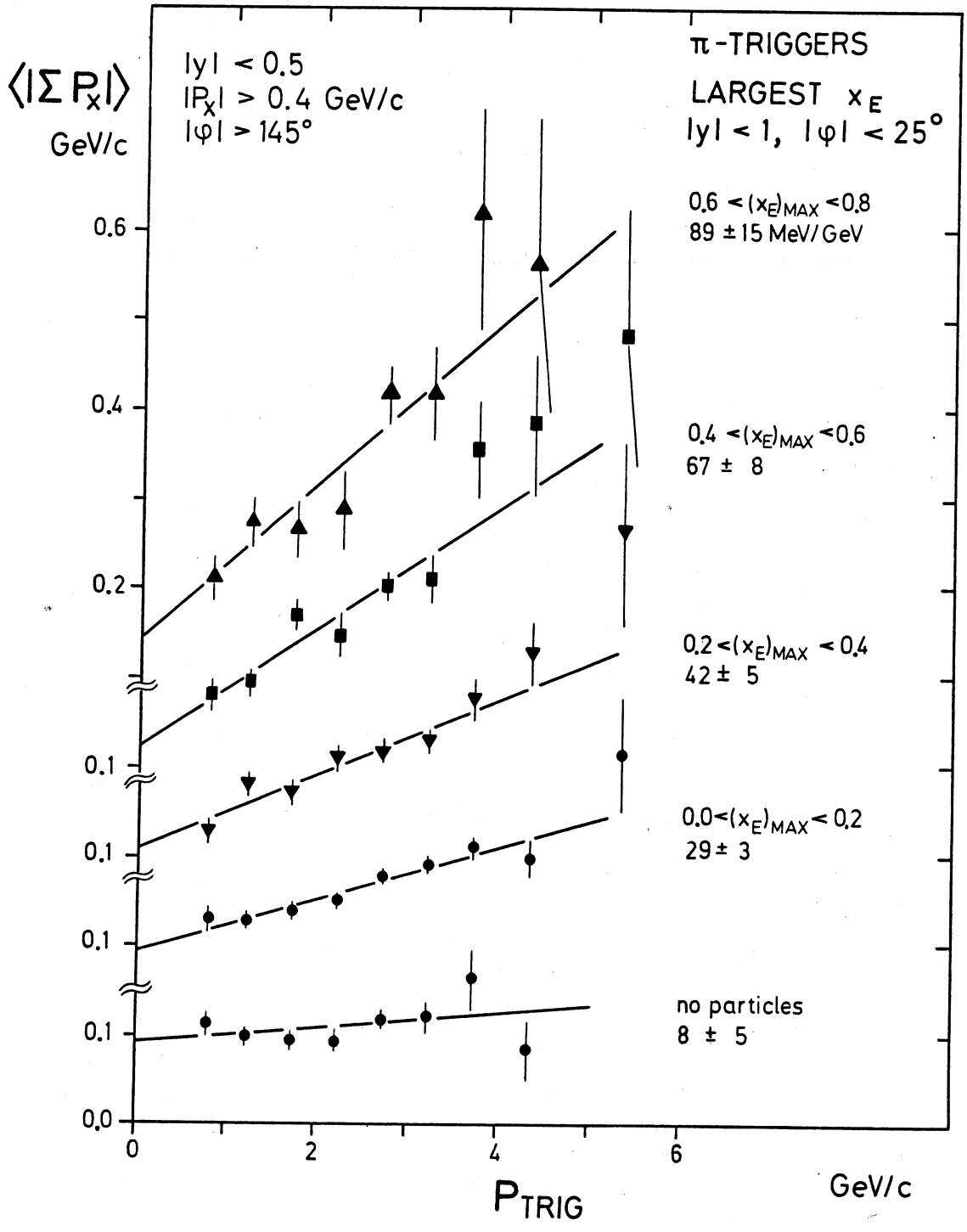
⟨|Σ Px|⟩
GeV/c
|y| < 0.5
|Px| > 0.4 GeV/c
|φ| > 145°
π-TRIGGERS
LARGEST xE
|y| < 1, |φ| < 25°
0.6 <(xE)MAX <0.8
89 ±15 MeV/GeV
0.4 <(xE)MAX <0.6
67 ± 8
0.2<(xE)MAX < 0.4
42 ± 5
0.0<(xE)MAX< 0.2
29 ± 3
no particles
8 ± 5
0.6
0.4
0.2
0.1
0.1
0.1
0.1
0.0
0
2
4
6
PTRIG
GeV/c

Fig. 24

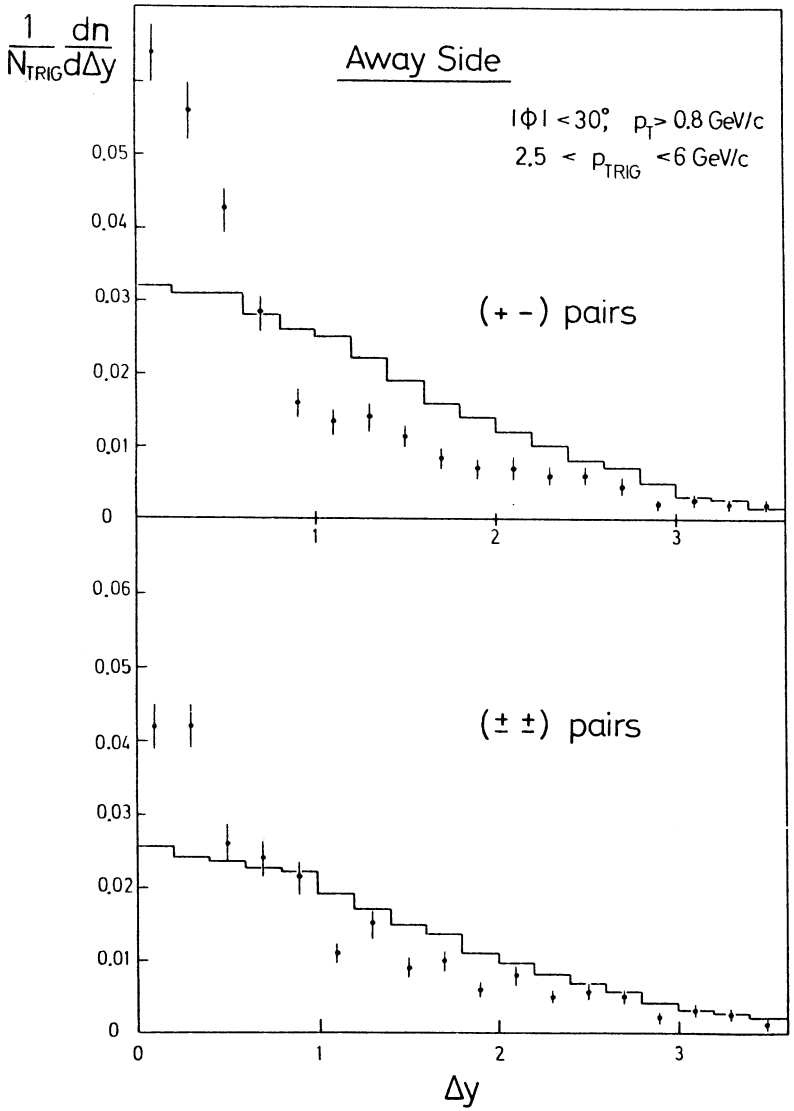
1/N_TRIG dn/dΔy
Away Side
|φ| < 30°, p_T > 0.8 GeV/c
2.5 < p_TRIG < 6 GeV/c
(+ -) pairs
(± ±) pairs
Δy

Fig. 25

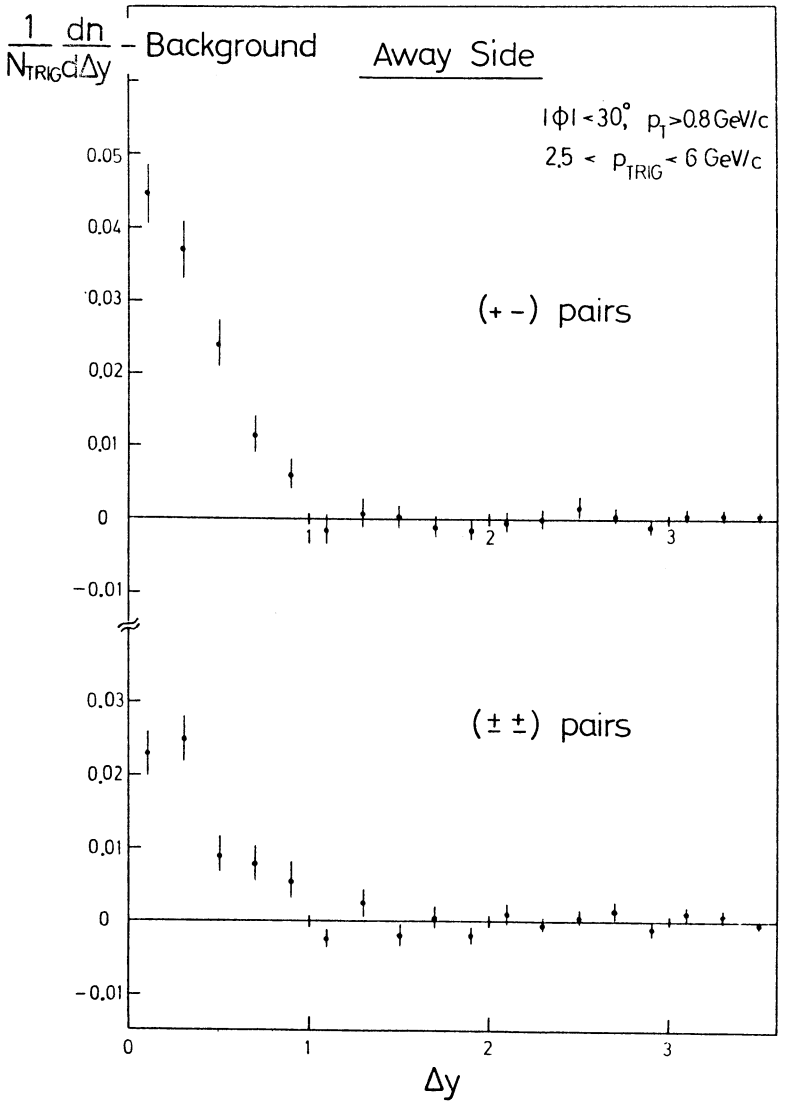
1/N_TRIG dn/dΔy - Background
Away Side
|φ| < 30°, p_T > 0.8 GeV/c
2.5 < p_TRIG < 6 GeV/c
(+ -) pairs
(± ±) pairs
Δy

Fig. 26

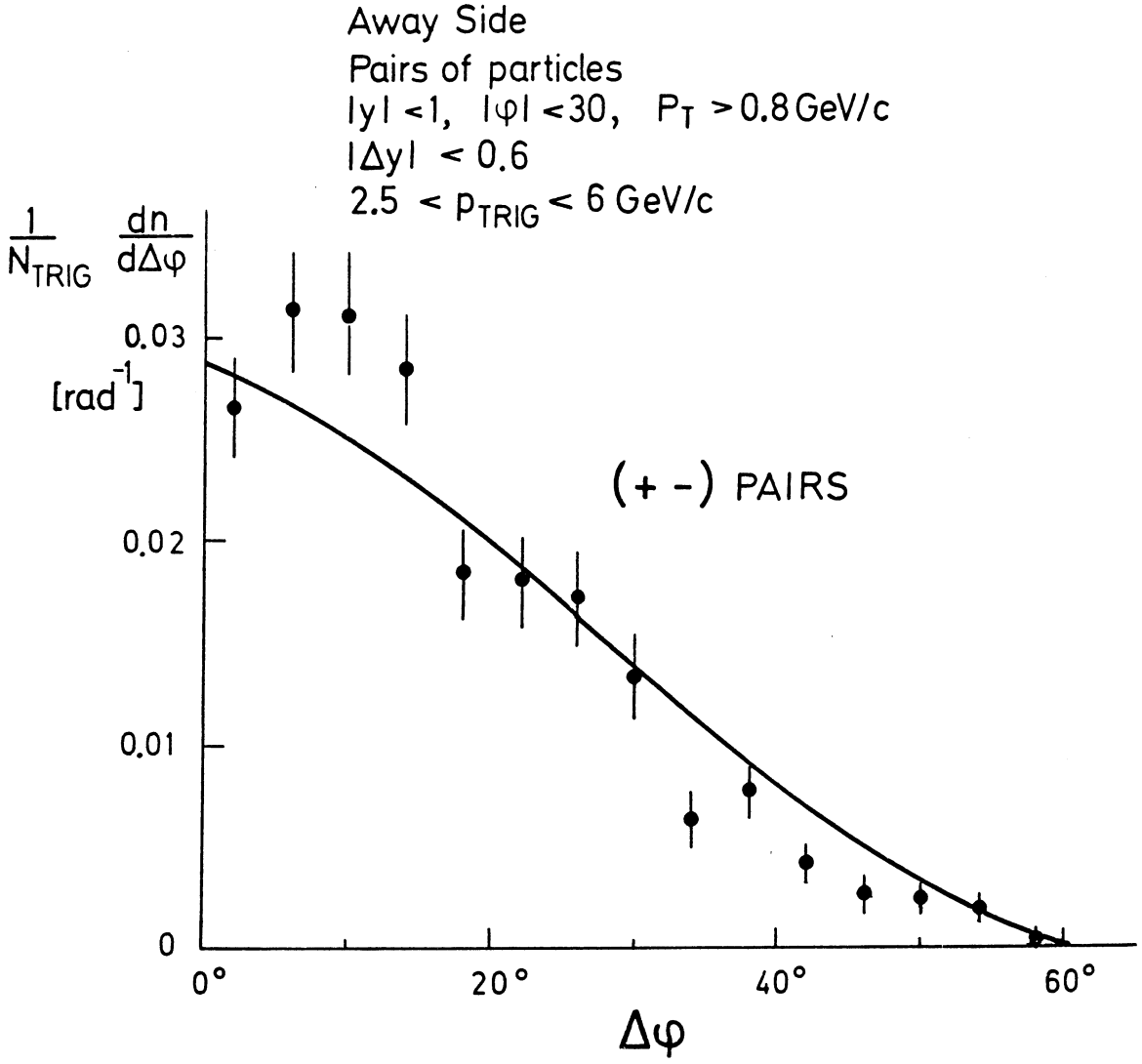
Away Side
Pairs of particles
|y| <1, |φ| <30, P_T >0.8 GeV/c
|Δy| < 0.6
2.5 < p_{TRIG} < 6 GeV/c
$\frac{1}{N_{TRIG}} \frac{dn}{d\Delta\varphi}$
[rad^{-1}]
0.03
0.02
0.01
0
(+ -) PAIRS
0°
20°
40°
60°
Δφ

Fig. 27

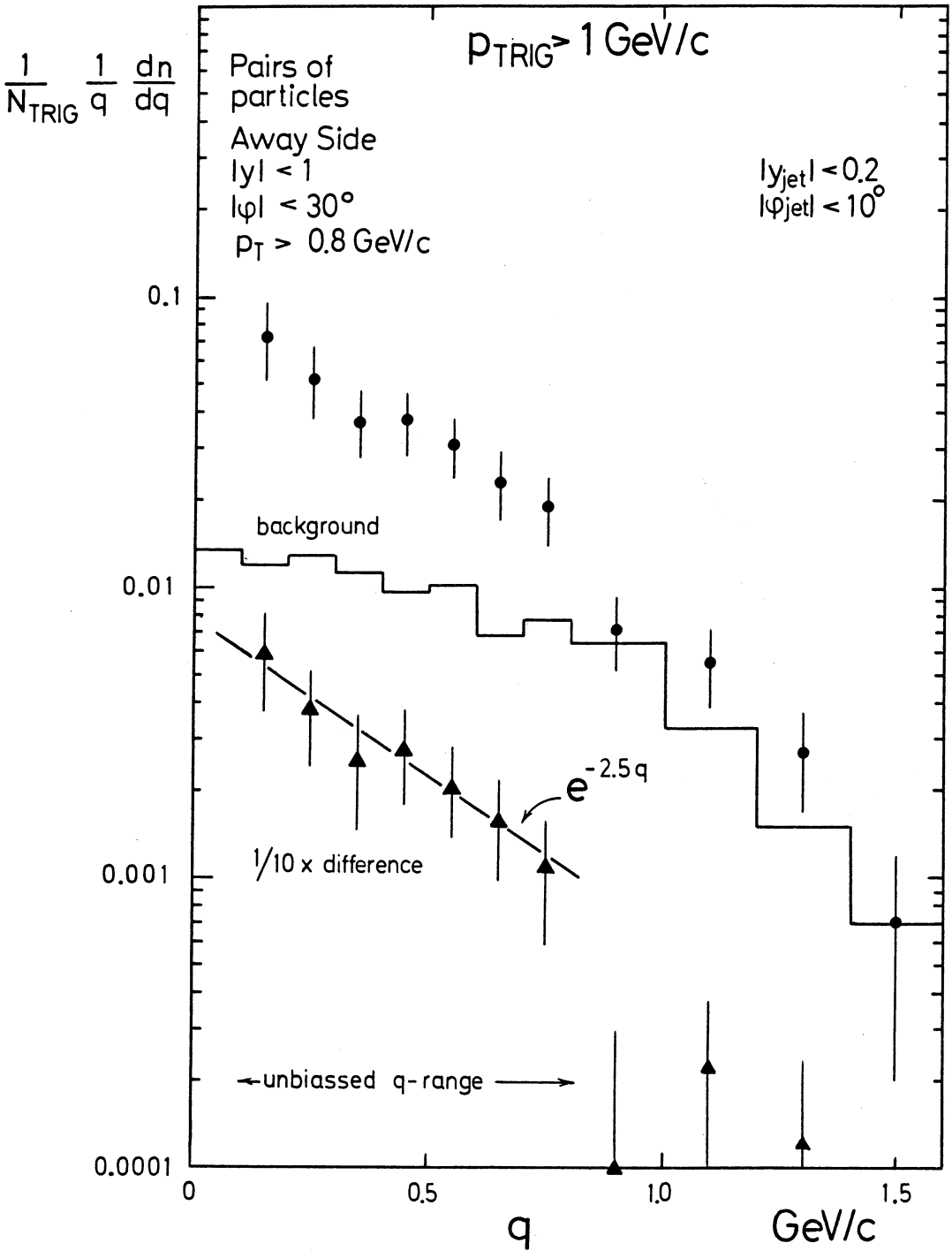
$\frac{1}{N_{TRIG}} \frac{1}{q} \frac{dn}{dq}$
$p_{TRIG} > 1$ GeV/c
Pairs of particles
Away Side
$|y| < 1$
$|\varphi| < 30°$
$p_T > 0.8$ GeV/c
$|y_{jet}| < 0.2$
$|\varphi_{jet}| < 10°$
background
$e^{-2.5q}$
1/10 x difference
unbiassed q-range
0.1
0.01
0.001
0.0001
0
0.5
1.0
1.5
q
GeV/c

Fig. 28

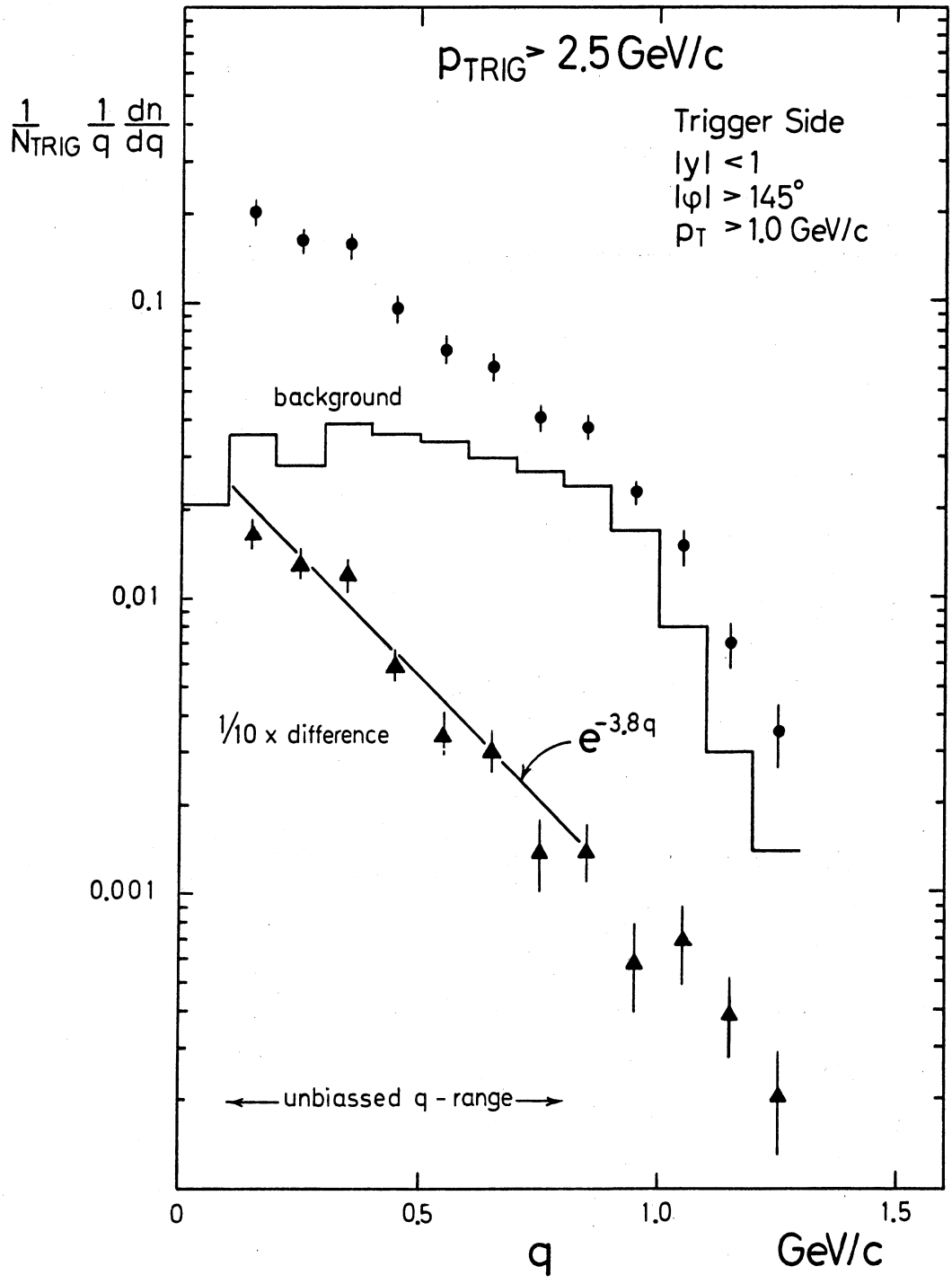
$p_{TRIG} > 2.5$ GeV/c
Trigger Side
|y| < 1
|φ| > 145°
p_T > 1.0 GeV/c
$\frac{1}{N_{TRIG}} \frac{1}{q} \frac{dn}{dq}$
0.1
0.01
0.001
background
1/10 x difference
$e^{-3.8q}$
unbiassed q - range
0
0.5
1.0
1.5
q
GeV/c

Fig. 29